NAVAL POSTGRADUATE SCHOOL

MONTEREY, CALIFORNIA

THESIS

SELECTIVE LASER MELTING OF BORON NITRIDE NANOPLATELET-REINFORCED TITANIUM COMPOSITES

by

Marian A. Jester

June 2021

Thesis Advisor: Andy Nieto
Co-Advisor: Walter Smith

Approved for public release. Distribution is unlimited.

THIS PAGE INTENTIONALLY LEFT BLANK

REPORT DOCUMENTATION PAGE			*Form Approved OMB No. 0704-0188*

1. AGENCY USE ONLY *(Leave blank)*	**2. REPORT DATE** June 2021	**3. REPORT TYPE AND DATES COVERED** Master's thesis

4. TITLE AND SUBTITLE SELECTIVE LASER MELTING OF BORON NITRIDE NANOPLATELET-REINFORCED TITANIUM COMPOSITES	**5. FUNDING NUMBERS**
6. AUTHOR(S) Marian A. Jester	
7. PERFORMING ORGANIZATION NAME(S) AND ADDRESS(ES) Naval Postgraduate School Monterey, CA 93943-5000	**8. PERFORMING ORGANIZATION REPORT NUMBER**
9. SPONSORING / MONITORING AGENCY NAME(S) AND ADDRESS(ES) N/A	**10. SPONSORING / MONITORING AGENCY REPORT NUMBER**

11. SUPPLEMENTARY NOTES The views expressed in this thesis are those of the author and do not reflect the official policy or position of the Department of Defense or the U.S. Government.

12a. DISTRIBUTION / AVAILABILITY STATEMENT Approved for public release. Distribution is unlimited.	**12b. DISTRIBUTION CODE** A

13. ABSTRACT (maximum 200 words)

Selective laser melting (SLM) is limited by the lack of composite powders available for purchase. This thesis focused on additively manufactured boron nitride nanoplatelet-reinforced titanium composites that maintain the structural integrity of traditional titanium alloys while promoting an increase in hardness and wear resistance. Boron nitride nanoplatelets (BNNP) were used as reinforcements due to their two-dimensionality and large surface areas. These properties aid in alloying with the spherical titanium powders without significant powder morphology. Titanium alloy (Ti-64) was researched to form a baseline of the properties expected and was used as the control. Titanium metal matrix composites (Ti-MMC) were produced using spatial arrays created using bulk Ti-64 mixed with Ti-BNNP composites forming regional microstructures. These spatial arrays consist of 0.5, 1.0, and 2.5 vol% composites with dispersions of reinforcement rich and reinforcement deficient regions. Each part was fabricated using SLM, and heat treatment took place upon fabrication to compare microstructure and porosity changes. Hardness testing and dry sliding tribological testing was performed to evaluate mechanical properties and wear resistance exhibited by Ti-MMC reinforced with nitrides. The addition of BNNP, even at low volume percentages (0.5 vol%), resulted in an increase of localized hardening with the max hardening increase of 36% (2.5 vol%).

14. SUBJECT TERMS additive manufacturing, bio-compatibility, titanium, nitrides, spatial arrays, tribology, wear, hardness	**15. NUMBER OF PAGES** 83
	16. PRICE CODE

17. SECURITY CLASSIFICATION OF REPORT	**18. SECURITY CLASSIFICATION OF THIS PAGE**	**19. SECURITY CLASSIFICATION OF ABSTRACT**	**20. LIMITATION OF ABSTRACT**
Unclassified	Unclassified	Unclassified	UU

NSN 7540-01-280-5500

Standard Form 298 (Rev. 2-89)
Prescribed by ANSI Std. 239-18

THIS PAGE INTENTIONALLY LEFT BLANK

Approved for public release. Distribution is unlimited.

SELECTIVE LASER MELTING OF BORON NITRIDE NANOPLATELET-REINFORCED TITANIUM COMPOSITES

Marian A. Jester
Lieutenant, United States Navy
BS, U.S. Naval Academy, 2014

Submitted in partial fulfillment of the
requirements for the degree of

MASTER OF SCIENCE IN MECHANICAL ENGINEERING

from the

NAVAL POSTGRADUATE SCHOOL
June 2021

Approved by: Andy Nieto
Advisor

Walter Smith
Co-Advisor

Garth V. Hobson
Chair, Department of Mechanical and Aerospace Engineering

THIS PAGE INTENTIONALLY LEFT BLANK

ABSTRACT

Selective laser melting (SLM) is limited by the lack of composite powders available for purchase. This thesis focused on additively manufactured boron nitride nanoplatelet-reinforced titanium composites that maintain the structural integrity of traditional titanium alloys while promoting an increase in hardness and wear resistance. Boron nitride nanoplatelets (BNNP) were used as reinforcements due to their two-dimensionality and large surface areas. These properties aid in alloying with the spherical titanium powders without significant powder morphology. Titanium alloy (Ti-64) was researched to form a baseline of the properties expected and was used as the control. Titanium metal matrix composites (Ti-MMC) were produced using spatial arrays created using bulk Ti-64 mixed with Ti-BNNP composites forming regional microstructures. These spatial arrays consist of 0.5, 1.0, and 2.5 vol% composites with dispersions of reinforcement rich and reinforcement deficient regions. Each part was fabricated using SLM, and heat treatment took place upon fabrication to compare microstructure and porosity changes. Hardness testing and dry sliding tribological testing was performed to evaluate mechanical properties and wear resistance exhibited by Ti-MMC reinforced with nitrides. The addition of BNNP, even at low volume percentages (0.5 vol%), resulted in an increase of localized hardening with the max hardening increase of 36% (2.5 vol%).

THIS PAGE INTENTIONALLY LEFT BLANK

TABLE OF CONTENTS

LIST OF FIGURES

LIST OF TABLES

THIS PAGE INTENTIONALLY LEFT BLANK

LIST OF ACRONYMS AND ABBREVIATIONS

AM	additive manufacturing
BN	boron nitride
BNNP	boron nitride nanoplatelet
COF	coefficient of friction
CP-Ti	commercially pure titanium
DMLS	direct metal laser sintering
HEBM	high energy ball mill
HIP	hot isostatic press
HT	heat treat
MMC	metal matrix composite
OM	optical microscope
SEM	scanning electron microscope
Ti-64	titanium-aluminum-vanadium
TiB	titanium boride
TiB2	titanium diboride
TiC	titanium carbide
Ti-MMC	titanium metal matrix composite
TiN	titanium nitride

THIS PAGE INTENTIONALLY LEFT BLANK

ACKNOWLEDGMENTS

I would like to acknowledge all my professors who helped guide me to my thoughts and equipped me with the tools necessary for this academic achievement. I would like to thank my advisors, Dr. Nieto and Dr. Smith, who sacrificed a lot of their valuable time and guided my research. Working with both of you has been a pleasure.

Secondly, I would like to acknowledge the staff at the MAE machine shop and Dr. Ansell, all of whom assisted me in sample preparation and characterization. Your patience and willingness to serve me as a student did not go unnoticed.

THIS PAGE INTENTIONALLY LEFT BLANK

I. INTRODUCTION AND BACKGROUND

A. TITANIUM AND BORON NITRIDE BIOMEDICAL APPLICATIONS

Titanium plays a critical role in biomedical engineering and is diversely used throughout the entire human body. Statistically, over 1000 tons of titanium and titanium alloy devices are used each year to support life [1]. Biomedical engineering, a field focused on supporting the human body when it becomes compromised, is continuously evolving. As life expectancy continues to increase, humans become more susceptible to deterioration, resulting in losing the body's full functionality. Biomedical applications can enhance the human experience by providing robust, reliable, and ergonomic devices that serve as an alternative to our natural anatomy. Metallic devices have a broad scope of uses in the dental, cardiovascular, and orthopedic fields, to name a few. Pacemakers, angioplasty stents, joint replacements, tooth spacers, and crowns, as shown in Figure 1, are all examples of biomedical devices that require different mechanical properties to function correctly.

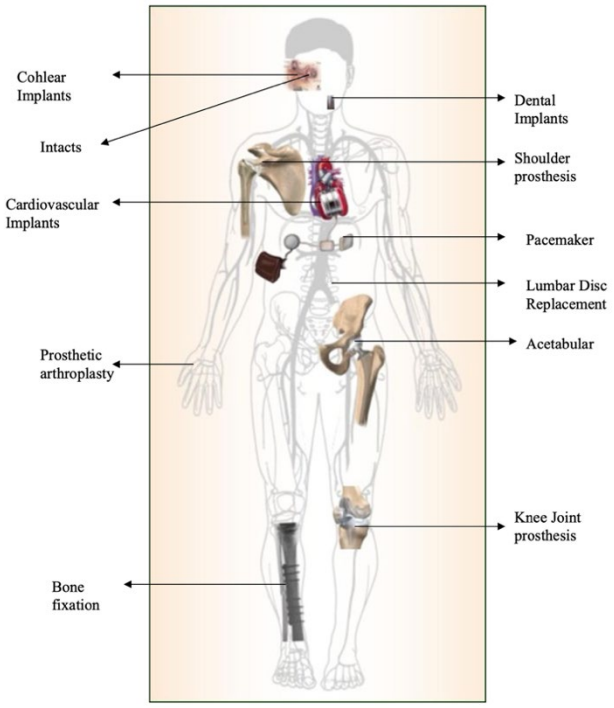

Figure 1. Titanium is used in various parts of the body. Source: [1].

Utilizing different fabrication methods and understanding the metals' mechanical limitations can help engineers determine the best suitable material and best manufacturing mechanisms.

1. Fields of Use

In the field of dentistry, titanium is used as the primary material for dental implants. These implants have to interact with bones and soft tissues providing a stable anchor and structural integrity to the prosthesis [2]. Orthopedic surgeons have used titanium and its alloys for several compact bone functions; however, commercially pure titanium (CP-Ti) does not meet the tensile strength requirements and titanium-aluminum-vanandium (Ti-64) has been shown to release toxic metal ions capable of damaging surround tissues [3,4]. The common practice is to use titanium in areas like the femoral necks and stems, which require a significant amount of strength but will not be susceptible to the same stresses as other locations [3]. As the human life expectancy increases and the population density of the elderly begins to rise, reliable bone alternatives will become pre-requisites to preserving the quality of life.

2. Biocompatibility

Titanium has been used extensively in the human body because of its natural corrosion and fatigue resistance. However, the typical titanium alloy used in the human body, Ti-64, alone, does not possess the properties necessary to protect again wear. Compared to commercially pure titanium, Ti-64 has less than desirable properties. Compared to bone, Ti-64 possesses a high modulus of elasticity and lower wear resistance. Extra-cellular reactions with the foreign material cause the metal to decompose and particulates to transport to different body areas [5]. Tests are conducted to determine if the mechanical properties of the metal are conducive for the environment it will be used in. Two testing methods are used in vitro and in vivo, the former being conducted external to a living organism and the later taking place within a living organism [1]. Upon being placed in the human body, the metal will experience continuous reactions with the tissues surrounding the implant. In vivo tests are conducted to gain an initial analysis of what potential issues could arise if the metal was implanted. By creating solutions like the expected host environment, in vitro tests can reduce

the risk of potentially dangerous reactions. For example, scientists can create artificial saliva in order to measure the risks involved with materials intended for dental use [6]. Similarly, in vivo testing using animals provides an actual example of the expected reactions that will occur without being exposed to the atmosphere which is essential to understanding the holistic properties of the material [1].

3. Corrosion Resistance

Titanium's anti-corrosive properties are a direct result of its surfaces being in contact with gaseous atmospheres [4]. Surface oxide layers form and, depending upon the thickness, act as a barrier that prevent wear and corrosion [4,6]. It has been found that by using thermal oxidation of titanium, the oxide layers can be increased and distributed uniformly, resulting in better protection for the material in its hostile environment [7]. For three days exposing titanium to higher heats 700ºC as opposed to 600ºC, in particular, Aniolek et al. [7] was able to produce an oxide layer, TiO_2, approximately three times as thick. In addition to the overall wear resistance, by increasing the oxidation layer, the overall hardness of the material is also increased [7]. Additionally, by changing the heat, you can change the material's hardness so the metal being utilized performs to its desired functionality. This relationship is why studying titanium metal matrices (Ti-MMCs) reinforced with ceramic particulates is essential. Corrosion and fretting can have many damaging effects on the human body. Eliaz et al. [6] determined that depending on the medium, corrosion can cause electrical disturbances that affect cell behavior, alter the chemical environment and even cause changes to our cellular metabolism. Bodily fluids concentrations of chloride, dissolved oxygen, and different pH levels are the characteristics that most often cause corrosion.

Boron nitride also has shown corrosion-resistant properties. Yi et al. [8] coated a polymer surface with boron nitride nanoplatelets (BNNP) and observed its response to oxygen-atom corrosion. This type of corrosion is more severe than atmospheric corrosion and further reinforced the relevance of the study by exposing the BNNP to atomic oxygen vice diatomic molecular oxygen [8]. They attributed the BNNP ability to protect the polymer membrane to BNNP's relatively large surface area, acting as a barrier that

prevents oxygen from entering the substrate via boron and oxygen bonding. Since the BNNP are bonded to the surface of the polymer, the oxygen interacts with the nitride layer but protects the polymer membrane substrate from the oxidation reduction corrosion mechanism [8]. This process was observed due to the coating of BNNP exhibiting signs of cracking and presenting a much rougher surface than before being exposed to the corrosive environment. A parallel to anti-corrosive paints can be drawn where the BNNP reacts with its environment to the benefit of the polymer its protecting.

4. Fretting

Titanium and its alloys can be very stable when placed in the human body due to the formation of the oxide layer; however, if that layer is depleted, the metals become susceptible to pitting and fretting [6]. Fretting, associated with load bearing parts, creates defects at points of contact and can cause premature cracking. The friction induced by the surfaces in contact causes increased shear stress and tensile stress, ultimately leading to mechanical vulnerabilities. Standard medical devices that experience fretting are the ball and joint hip replacements because they will have steady contact and experience cyclic stresses [6]. When titanium is fabricated to remain porous, it becomes more susceptible to pitting and crevice corrosion. The decrease in density directly impacts the oxidation-reduction reactions of metals, which causes pH levels to become very acidic [6]. Some of the titanium alloys, including Ti-64, have been shown to release metal ions that contaminate the human body [2–4,6]. When the natural oxide layer that Ti-64 creates depletes, vanadium can diffuse into the surrounding tissues and creates sites for corrosion to form. Galvanic coupling, a process in which two metals interact, changing one into a cathode and the other into an anode, is widespread when pure titanium and its alloys are connected due to bodily fluids acting as the electrolyte [6]. The couple concomitant with CP-Ti and other Ti alloys have been observed to cause corrosion in up to 35% of cases studied [5]. The galvanic couples and regional wear accelerate the corrosion process. Studying how ceramics increase wears resistance will prove beneficial to also reducing corrosion. Testing to ensure adequate protection against these degradations is vital to the overall understanding of prosthesis longevity.

B. ADDITIVE MANUFACTURING

1. History

Traditional manufacturing methods are known as subtractive manufacturing. By using machines like computer numerical control (CNC), a bulky piece of metal is cut to fabricate the desired shape, leaving behind shards of scrap metals. In the 1980s, a state-of-the-art concept called stereolithography emerged where 3D products could be produced based on depositing thin layers of materials. Stereolithography catalyzed change, allowing 3D structures to be created using 2D parameters. In its infancy, stereolithography was only used to produce parts using ultra-violet light sensitive polymers fabricated using lasers; however, as the technology gained traction, a diverse spectrum of uses began to emerge [9]. By 1992, companies began experimenting with metal AM, introducing a method known as laser sintering, and by the mid-2000s stainless steel, aluminum, cobalt-chrome, and titanium were all relevant within the AM industry.

2. Direct AM

Additive manufacturing comes in many different forms: direct energy deposition, sheet lamination, binder jetting, and most importantly, powder bed fusion, which will be the method examined extensively throughout this study. The powder bed fusion process entails constructing a part by fusing molten metal powder a single layer at a time, known as selective laser melting (SLM) [10]. Figure 2 represents an infographic that is listing the various components that are relative to the building process. Before melting the powder, various parameters like layer thickness, scanning speed, and the power the laser emits to melt the powders can be manipulated to influence the print's desired outcome [11]. The manufacturing process occurs in an environment that is very controlled. The amount of gas inside the printer (argon in this case), the build plate's temperature, and the overall print environment's temperature remains constant to reduce oxidation and any additional thermal stressing. By having exceptional control over the parameters in which a part is being produced, processing constraints can be reduced, and customized products can be manufactured to the exact functional specifications the client desires—enabling a paradigm shift from manufacturing almost exclusively in large factories to more bespoke ways of sourcing.

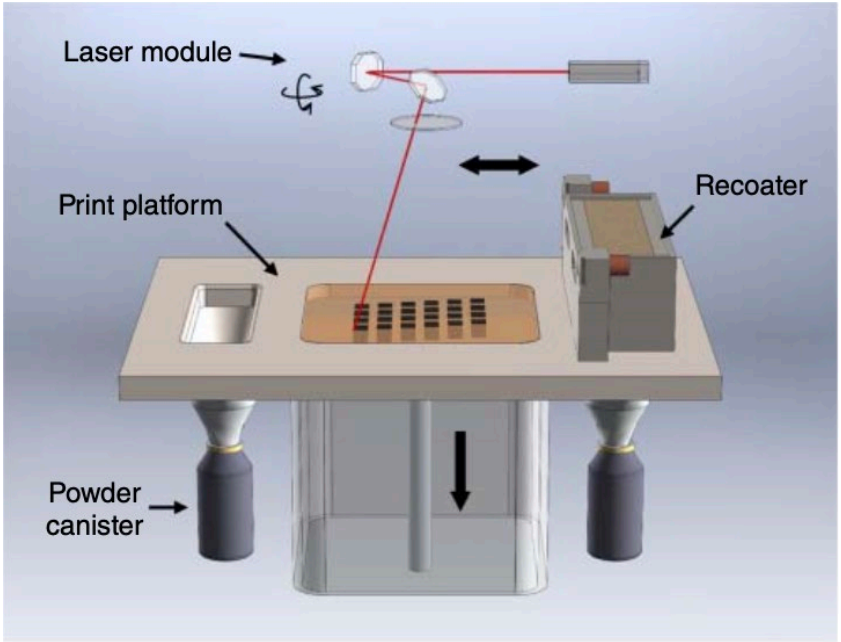

Figure 2. SLM printer diagram showing the major components Source: [12].

C. BENEFITS

1. Precise Designs

Creating parts is streamlined because of this novel manufacturing process. Rapid prototyping of parts with complex geometries are manufactured efficiently, rapidly, and at potentially lower labor costs due to their "set it and forget it" capability. The high level of resolution of each part is made possible by printing parts using computer-aided designs (CAD) [12]. These software files are then printed from a medium of choice to precise tolerances while maintaining their mechanical properties. It is unequivocally proving its potential to be utilized as a method of mass-producing parts or producing spare parts that typically require long lead times. The diversity of industries that this process can impact extends beyond rapid prototyping companies. AM is now established as relevant in the private, government, commercial, and academic sectors because of its future potential.

2. Waste Reduction

Manufacturing titanium alloys using subtractive manufacturing is a costly, inefficient process, especially when fabricating complex designs [13]. During AM, raw

materials are contained within a closed-loop system allowing the discarded powder to be collected and filtered, decreasing the amount of waste, and causing a cost reduction. Recycling these powders, too, serves to decrease the energy expended for production. By contrast, subtracting manufacturing results in an abundance of scrap metal that will likely require a tremendous amount of energy to recycle the waste material and return it to a usable product. Due to the nature of parts being generated from computer files, the potential to make modifications in real-time is possible, and manufacturing parts with different processing parameters with a push of a button eliminating the need to acquire new hardware like casts and dyes. Post-processing can also be reduced or eliminated in its entirety. The lack of post-processing needed upon completion of a build is also essential to decrease the amount of time required from build to consumer [10].

3. Military Use

The potential to introduce additively manufactured parts would provide an opportunity to circumvent the traditional supply chain delays and provide on-site production to optimize military readiness. This capability does not come without its challenges. In 2012, the U.S. government expressed specific interest in advancing additive manufacturing and other innovative manufacturing methods. Government funds were disseminated with the idea of using academic and other government entities to pursue research and development. Military standards, especially in the sea-going communities, demand very high standards in terms of mechanical properties. The nature of their corrosive operational environment parallels can be drawn between these parts and biomedical devices. Equipped with a 3D scanner, parts can be rendered and printed on-site to meet the demands for temporary and permanent fixes depending upon the piece of equipment. Depressurizing the logistical channels and getting service members the tools necessary to not only operate but thrive.

4. Commercial Use

The commercial sector has extensive uses for additive manufacturing. Metal matrix composites, used for their inherent inertness, can be created for the automotive and aerospace industries [14]. The original use of 3D printers was to perform rapid prototyping.

Perhaps on a smaller scale, companies could produce preliminary designs before committing to the final product. Prototypes and replacement parts that typically would expend an exuberant amount of money and energy could now be produced additively, with high precision. Precision designs are vital and many industries, especially biomedical and aerospace communities, where the margin of tolerable error is minute.

D. CHALLENGES

1. Scalability

Despite the many advantages of AM regarding extensive customization benefits available when prototyping on a small scale, fabricating parts on a large scale will likely prove challenging. The layer-by-layer approach of manufacturing induces more margin for defects and errors to be introduced into the system. This anisotropic behavior causes distortions in mechanical properties associated with the size, shape, and complexity of the structure and the volume of products being produced [13]. These same variables also affect the speed at which parts can be produced. Powder availability will also be a crux. The feedstocks available are dwarfed by the amount of MMC already being used via traditional methods. Later, this paper will discuss powder metallurgy to overcome this costly and time-consuming obstacle.

2. Post-processing

Post-processing can be a time-consuming venture and be accompanied by high costs. Upon the completion of an AM part, the part is not necessarily ready for use. Despite producing parts that do not require assembly, the parts still need to undergo some sort of milling to remove the support structures required to maintain stability [13]. Once removed, post-processing often is necessary to remove the manufacturing defects. Typically, titanium parts have a smooth finish; however, depending upon the AM used the parts could be very porous or have poor surface finishes [13]. Depending upon the intended field of use, different post-processing procedures can alter the parts' mechanical properties. Hot isostatic pressing (HIP) uses pressure and heat as a mechanism to sinter the part eliminating manufacturing defects like unintended pores and promoting densification [2,3].

3. Osseointegration Challenges

Biocompatibility will prove to be a major driving factor for the sustainability of AM parts for biomedical applications. When developing new metals, mechanical properties must be maintained without adverse effects from being implanted inside organic material. Titanium is used widely throughout the medical field, but it takes a very long time to integrate into the human body. For this reason they sometimes have to use coatings to speed up this process, which is not ideal because that requires more time after manufacturing the part [6]. Stress shielding, a biomechanical defect resulting from significant moduli differences occurs when titanium by itself is used on load bearing implants [10,15]. When coupled with low moduli bones, the stress shielding phenomenon could occur unless preventative measures are put in place to control the moduli disparity. If mechanical properties are not optimized, additional surgeries may be necessary to correct the deficiency induced by inadequately fabricated parts, causing unnecessary risks to the patient.

Surface roughness will likely play a major role in the biocompatibility and proliferation of cell growth. Ponsonnet et al. [16] determined surface roughness effects how cells to proliferate when in contact with biomaterial surfaces. Titanium, depending on the method of fabrications can vary in its surface roughness. Although this thesis will not conduct any analysis of the biocompatibility of the manufactured Ti-MMCs, future studies could be performed to bolster the legitimacy of using SLM to produce boron nitride reinforced composites for biomedical applications.

E. POWDER PROPERTIES

In the 1980s powder metallurgy (PM) was developed to keep fabrication costs to a minimum, as well as to provide a means of fabricating parts using metal matrix composites (MMCs). The PM process takes bulk powders and reinforces them with other powders to change the physical properties. Particular attention is paid to the number of reinforcing particles that will be the driving force for modifying and tailoring mechanical properties. Then, the powders are compacted into molds, sometimes requiring binders to retain its intended shape. The molds are then referred to as “green bodies” and are held together by

the compaction alone [17,18]. The molds are then sintered at a set temperature. This process requires a delicate balance to be maintained between temperature and duration of sintering. These parameters turn the fine powders into molten metal, and any powder that remains unsintered could result in cracking or other mechanical discrepancies [10].

Powder reinforcement has been studied for decades. Depending upon the reinforcing agent, this mechanism can provide favorable physical advantages. Typically, discontinuous metal matrices (DMMCs) reinforced with ceramics benefit from the ceramics' inherent thermal, wear, and hardness properties [19]. The ceramic that is providing the particulate reinforcement enhances the mechanical properties isotropically. Assuming the particulates are homogeneously distributed, the ceramic mechanical properties should remain consistent throughout the structure. However, the potential of particulates being inhomogeneously distributed, or lacking a consistent spatial orientation, could interfere with guaranteed structural integrity [19]. Objectively, using MMCs will promote direct strengthening caused by the ceramic bearing much of the load. When using metal matrix composites, the mechanical property disparities, like elastic modulus differences, between the metal and ceramic particulates causes stresses based upon how the composite is distributed. The ceramics added to the metal matrix possess properties that restrict expansion, unlike its metallic counterpart known as coefficient of thermal expansion. Knowing this value reveals how a composites mechanical properties will be changed as a result of thermal expansion and whether the MMC display any incompatibilities [20,21].

F. THESIS OBJECTIVES

AM is still in its infancy; the objective of this thesis is to synthesize Ti-MMC with BNNP as the reinforcing agent and evaluate how composition effects microstructure, hardness, and wear resistance. Powder synthesis methods and the formation of spatial arrays, will be studied to further understand the effect large volumes of BNNP will have on AM compatibility. The relationship between reinforcement rich and deficient regions will be evaluated to ascertain how spatial arrays effect toughening and what mechanisms contribute to variations in hardness and wear resistance.

II. ADDITIVE MANUFACTURING OF TITANIUM METAL MATRIX COMPOSITES OVERVIEW AND STATE-OF-THE-ART

A. MATERIAL PROPERTIES

1. Cerium Oxide

Since the early 1970s, nanoceria and their properties have been studied as a means to replace already existing technologies such as catalytic converters in the automotive industry and as a means to absorb ultraviolet rays [22]. The crystal structure associated with cerium oxide is composed of oxygen ions surrounded by cerium ions referred to as a cubic fluorite crystal structure [23]. Each of the oxygen ions is used to occupy all the tetrahedrons vacancies, which contribute to its biocompatibility, while the cerium ions occupy the vertices and faces [23,24]. The oxygen ions within nanoceria play an essential role in creating anti-inflammation by using the surface volume ratio as a means of creating free radicals that inhibit oxygen reactivity [22]. Essentially, the oxygen ion oriented at the surface of the nanoceria control the way electrons interact with cells and prevent structural damage [22]. These "free radicals" allow for additional bonding, resulting in neutralizing potentially damaging charged particles that cause inflammation. This reaction occurs when exposed to oxygen as standalone element cerium is not readily soluble in water, reducing the risks of toxicity but does not allow for its desired biological properties to be catalyzed [24]. Past studies have shown that cerium oxide has anti-microbial, anti-inflammation, and many different toxicity applications within the biomedical field. How the nanoceria is made also determines the surface properties. For nanoceria, calcination to remove impurities can change the specific area and presence of active sites [25].

2. Boron Nitride

Boron nitride (BN) has been used as a reinforcement because of its chemical inertness at high temperatures and mechanical properties. These properties come as a function of the way the nitride is bonded. Kostoglou et al. [26] notes that in its most stable form, hexagonal or h-BN is covalently bonded and structurally analogous to graphite [26]. They also mention surface area plays an important role in the functionality of BNNP as a

reinforcing particle [26]. Using its large surface area, BNNP can form a barrier layer which acts as an oxidation inhibitor [8]. Additionally, surface area will effects its thermal stability and change the temperature ranges it can perform as a barrier [26]. As mentioned BNNP are an analog of graphene nanoplatelets. As such, it is to be expected that some of the mechanical and material characteristics would coincide with its two-dimensionality; mainly, lubrication, thermal conductivity and enhancements in toughness would be expected [27].

B. POWDER

1. Powder Fiber Reinforcements

How MMCs are reinforced is fundamental to enhancing its properties. The mechanical differences between the metal and ceramic particulates can cause stresses atypical to an alloyed material. Inherently, ceramics tend to restrict expansion unlike its metallic counterpart. However, since Ti-64 already possess superior tribological and hardness properties, introducing a new ceramic may further improve upon those properties [28]. One way to reinforce a matrix is by discontinuously reinforcing the composite with particulates as show in Figure 3.

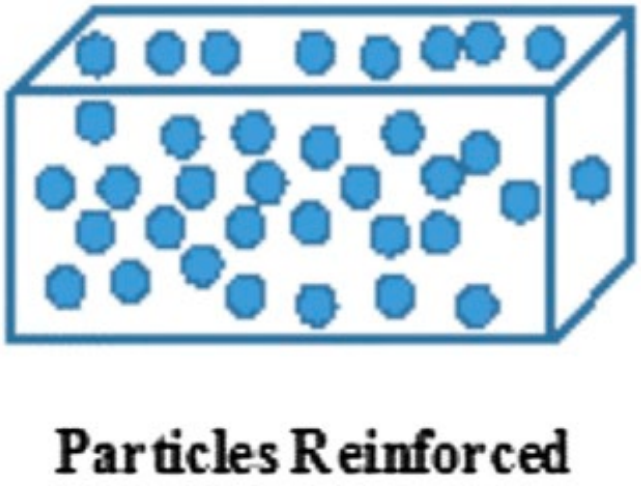

Figure 3. Diagram of particle reinforced parts. Source: [14]

Previously, DMMC were mentioned as a means of creating an isotopic mechanical advantage. DRTCs in particular, have been reinforced with borides [29], nitrides [28] and carbides [30] but some of these Ti-MMCs utilized a different reinforcing powder to form a desired in situ reaction [30,31]. A variety of particulates have been used to reinforce composites, all with different mechanical proprieties in mind. DRTCs have been studied on numerous occasions using different AM methods demonstrating tribological properties that exceed that of normal titanium alloys. Gu et al. [30], reinforced Ti-64 with SiC with the expectation of forming an in-situ TiC phase and studying its mechanical advantage. They were able to confirm hardness increases by more than 300% and a stark reduction in COF values from its control sample, Ti-64.

2. Powder Morphology

High energy ball milling (HEBM) is a method used to alloy particles together. Both powders are contained within the same canister, in which, balls are added as the mechanism for alloying the powders. The high energy collisions that occur disperse the powders and create homogenous distributions simultaneously [32]. As a result of the high energy of each collision, phase and morphology changes can be an unfortunate biproduct as shown in Figure 4 [32].

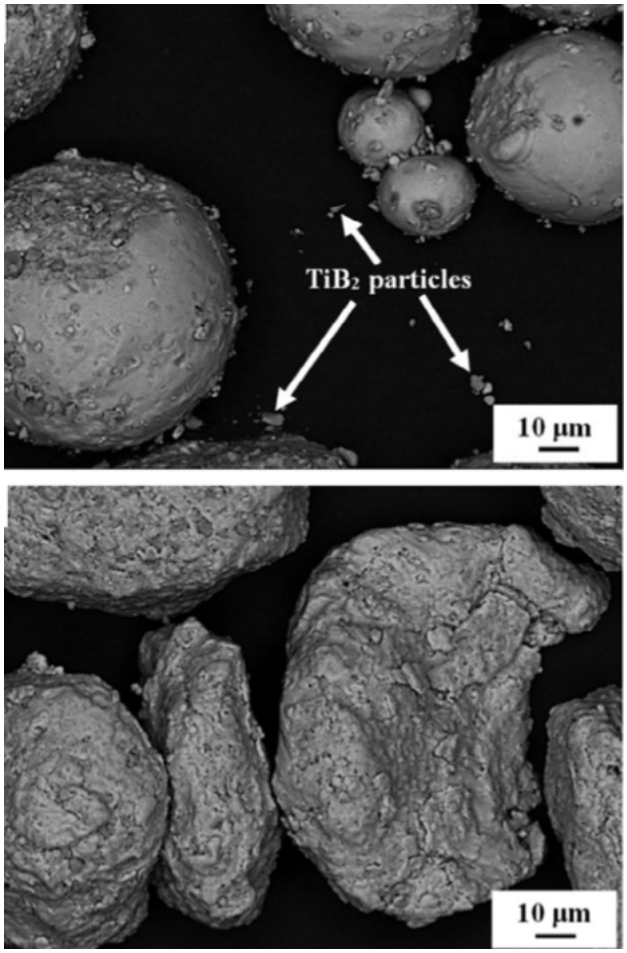

Figure 4. Powder Morphology of CP-Ti and TiB_2 ball milled for 1 hour (top) and 3 hours (bottom) Source: [33]

As stated previously, SLM works best when the feed stock powder is spherical. Powder morphology, the physical characteristics of the powder i.e., shape and size, contribute to density and how well the powders will perform via SLM [34]. Studies have been conducted, indicating that shape changes are inevitable but can be managed and become trivial if optimized [10,32,33]. Attar et al. [33], noticed that when creating a Ti-TiB_2 MMC 2 hours of milling was most appropriate for mixing to enable a uniform distribution of reinforcing particles. A reduction or increase in time spent milling either deformed the shape of the CP-Ti or left uncoalesced particulates. Using the exact same Ti-MMC, Zhang et al. [10], also concluded that 2 hrs. of milling resulted in the most optimal

properties. Other researchers have been able to develop homogenously alloyed Ti-MMC as well using milling [32,35,36].

3. Flowability

Despite the appeal, an additively manufactured part is only as good as its single layer. Producing a part layer by layer incorporates complexities not seen in traditional manufacturing. Physical phenomenon present throughout the process carries elements of laser attenuation, heat transfer, phase transformation, the flowability of both the powder and the melted derivative, and various other reactions causing stressing. Residual stresses are a common challenge when using additive manufacturing. Preheating the powder prior to printing is beneficial by decreasing the thermal stresses associated with the laser interacting with a significantly colder powder. Preheating the powder also allows for the powders to flow better, resulting in a more uniform powder layer for the laser to engage, this paper will delve further into flowability as it relates to spreadability later. The objective is to produce a part that is dense and free of irregularities like voids and pockets of unmelted powders. Often, pores result as the powder is unevenly distributed or melted, creating defects that can lead to crack propagation [10,13]. In addition, selective laser melting can cause balling to occur, leading to the obstruction of the recoater blade's path. Obstructing the recoater's path causes uneven powder deposition and deformation in the structural shape [11]. By association, homogeneity is compromised, should these challenges not be overcome leading to inconsistencies between parts that could result in distorting the material properties expected.

C. FABRICATION

1. Energy Densities

Energy density plays an important role in the fabrication of each part. When a MMC is used with the Ti-64 standard configuration, the energy density used for the print does not consider the reinforcing particulates. Thus, causing disturbances in the build process if the powder goes unmelted or melts disproportionately. To compensate, processing parameters can be changed to reduce the likelihood of such effects. Equation 1 describe in

Zhang et al. [10] shows energy density as a function of hatch laser power [P], hatch spacing [s], scanning speed [v] and thickness [t] in relation to the distance to the build plate.

$$E = \frac{P}{v*t*s} \quad (1)$$

Yadroitsev et al. [11] studied the effects of energy density on single tracks using a variety of feedstocks and laser parameters. The purpose of their study was to determine the ideal energy density to fully penetrate the substrate while maintaining consistent geometric melting geometries throughout the build. Regardless of the feedstock, how the powders melted corresponded to the laser inputs. With regards to scanning speed, it was observed that too high scanning speeds caused balling, whereas slower speeds led to inconsistent tracks, attributed to the thermal conductivity of the metal. Other studies [10,28] focused on studying energy densities to understand how they could change the mechanical properties of composite. By changing the energy density, a different thermal history is generated leading to the formation of different microstructures. For instance, Zhang et al. [10] observed that by increasing temperature gradients, as a result of increasing scan speeds the change in cooling effect leads to α' forming instead of the typical α phase for CP-Ti. Likewise, Kundu et al. [28], reinforced titanium with TiN by DMLS, using various scan speeds and laser power to study hardness and wear resistance. For all hardness and wear tests conducted, the specimen associated with the highest energy density, consistently showed improved wear resistance and hardness properties.

2. Heat Treatment Effects

As mentioned, one of the benefits of AM is its efficiency. Fabricating parts without the requisite of post-processing. However, when coupled with post-processing methods, like heat treatments as-printed parts could see added benefits. Fousova et al. [37] printed Ti-64 parts and annealed them post print. Their method used different atmospheres (vacuum, argon, and air), a temperature of 820ºC for 90 minutes, a heating rate of 200ºC per hour, and the parts were cooled in the furnace until 500ºC, followed by air-cooling until room temperature. When using Ar^+ as the process gas they observed a maximum in hardness increase, but they concluded this was a result of oxygen entering the intestinal

voids of the substrate and a small oxide layer being formed [37]. Roudnicka et al. [38] focused on different types of heat treatments and the mechanical property changes associated with each. The microstructures and porosities of parts post-processed using hot isostatic pressing (HIP) and standard heating in argon were compared to determine how each part is influenced by temperature and pressure variants. They found that when HIP was used, less pores remained however, the material was not as hard as the standard heated parts. Many researchers have all discovered that heating caused microstructure changes and a reduction in porosity [37–39].

3. Microstructure

Many factors contribute to the microstructure developed in an AM part. Powder type, energy density and post-processing procedures will affect the microstructure because chemical composition of the powder and its lattice structure determine crystallographic details like spatial orientation and how grain boundaries will form when the metal is melted. Titanium, in its α phase is an HCP structure, as a result this phase provides strength but brittleness because HCP does not have many slip systems to allow for dislocations [36,40]. These slip systems act as a medium on which the grains can alter position because of an external force. The more slip directions a material possesses the more the material can move on a microscale and in turn the greater ductility. Conversely, titanium also exists in body centered cubic when it is in its ß phase.

Ti-64 is an α+ß alloy, suggesting that when melted, the molten metals recrystallization process should yield a combination of grains representative of both phases. When SLM is performed a martensitic α' phase is formed and the α phase may be non-existent [41,42]. To recover different phases post-processing heat treatments can be used. For example, Vrancken et al. [42] conducted a study to identify the influence temperature has on the formation of microstructures. With the understanding that the ß transformation temperature is at 995^{o}C for Ti-64, they performed heat treatments above and below this threshold to assess the changes in microstructure. As expected, heat above the ß transition temperatures allowed more α phase to be produced as a result of rapid grain growth [41]. In a later study they conducted in 2015, they also determined that when they

used a Ti-MMC they were able to change the ß transition temperature allowing for phase changes at a lower temperature [42].

4. Mechanical Properties

The mechanical properties of Ti-64 composites differ in relation to the processing parameters. This is a result of the different microstructures that form when the laser power is being manipulated as well as the melt pool geometry [43]. Zhang et al. [10] conducted a 2015 study that found, in some cases, mechanical properties could be superior to those of traditionally manufactured parts. Specifically, hardness when manufactured using SLM increased by almost 20% over the same part that was manufactured by casting [10]. Which could be advantageous because the hardness of bone is very low compared to metals having a Vickers hardness (HV) of 26.3 [5]. Other studies have also found similar results, showing that wearability is also improved by using Ti-64, which by itself promotes a decrease in wearability [28]. When coupled with various ceramics as reinforcements these properties could increase even more.

5. Wear Resistance

High wear resistance is a requisite for metals entering an organic environment. Although titanium possesses great corrosion resistance, as a result of the formation of the oxide layer, its wear resistance is subpar to its alloys [6]. Ti-MMC has exhibited a significant wear resistance because they are reinforced with ceramics that are inherently harder than titanium alone. AM of Ti-MMCs could play an important role in finding alternative solutions to manufacture parts at lower costs.

Cai et al. [36] conducted a study using Ti-MMC reinforced with borides intending on identifying the mechanical and microstructure transformation associated with the in-situ and ex-situ formation of composites. Using TiB_2 as the nano reinforcement they observed the tribological and hardness changes as TiB formed in-situ, attributed to:

1. In-situ phases thermodynamic stability
2. Clean interfacial bonding
3. The uniformly distributed finely grained reinforcement particles [36]

Ultimately they concluded that the wearability was a direct correlation to the improved hardness [28,36]. Kundu et al. [28], found very similar results when nitrides were used to reinforce Ti-64 they found a coefficient of friction reduction as more reinforcement volume was used, decreasing 0.65 for Ti-64 down to as low as 0.33 when 15 volume percent of TiN was used [28]. Furthermore, TiN a reinforcement also increased wear resistance and microhardness tests showed improvements [28]. Also important to note is that as power was increased, the densification of each specimen, regardless of the volume of ceramic added as a reinforcing agent also showed an increase [28]. Attar et al. [33] used a mix of commercially pure titanium and TiB_2 (titanium diboride) showing a consensus that microhardness and wear resistance are improved, regardless of the reinforcing ceramic [33].

THIS PAGE INTENTIONALLY LEFT BLANK

III. MATERIAL DESIGN OF BORON NITRIDE AND TITANIUM ALLOY SPATIAL ARRAYS

A. FABRICATION OF BORON NITRIDE REINFORCED TITANIUM COMPOSITES

The Ti-64 powder used to fabricate all parts was explicitly made for the manufacturer's EOS 100M SLM machine. The chemical composition meets ASTM F2924 standards, and the particle size is reported as ~39-microns. However, the manufacturer recommends sieving the powder through a 63-micron filter to remove any larger agglomerates that may have formed post packaging. Additionally, the manufacturer reports the particle layer thickness of the Ti-64 powder to be ~20 microns with a density of 4.4 g/cm^3.

The BNNP was procured via Sky Spring Nanomaterials Inc., located in Houston, TX, USA. The nano powders have a hexagonal crystal structure, are ~100 nm in diameter, and possess a density of 2.1 g/cm^3.

1. Composite Powder Synthesis

The Ti-BNNP composite powders were created using HEBM. As mentioned in Chapter II Section B Part 3, HEBM is a standard method used to make MMCs. Parameters were chosen with the intent to maintain the spherical integrity of the Ti-64 bulk powder, promote a homogenous distribution of the reinforcing BNNP, and ensure the majority of the BNNP coalesced to the surface of the Ti-64 particles. To do so, different volume ratios of titanium composites were created by adding 2% and 5% by volume of the BNNP to the Ti-64 bulk powder. These powder mixtures and steel balls were then added to the steel canisters at different ball ratios corresponding to weight. The ratios used were 2:1, 1:1, and 1:2, where the numbers represent the ball and powder weights, respectively. The canisters were then placed in the SPEX Sample Prep Mixer/Mill 8000D, capable of mechanical alloying and nano-milling simultaneously. The balls were milled for 80 minutes using a four-minute mixing and a five-minute stagnation period between sessions. This interval was used to allow the heat to dissipate and mitigate the possibility of carbides like TiC

forming from the steel balls interacting with the Ti-MMC composite powder. Upon completion, the coalesced powder was removed and sieved through a 45-micron filter before forming the spatial arrays.

After milling was complete, spatial arrays were formed using the newly developed Ti-MMC and Ti-64. Jiang et al. [44] developed a method to engineer spatial arrays that promote toughening by distributing stress concentration areas and having areas that vary in hardness [44,45]. Distributing a composite throughout a bulk powder randomly results in regions that contain different mechanical properties. The desired outcome was to produce composite rich regions and composite deficient regions uniformly dispersed throughout the matrix. Toughening is influenced by particle size, morphology, and the MMC concentration distributed throughout the bulk powder [44,45]. Three different powder compositions were created, shown in Table 1 powders B and C were formed via a 50/50 mixture of Ti-64 and Ti-MMC, whereas powder A was reduced twice, once to form 1% and again to form the Ti-0.5BN composite, desired. After each mixture, the powders were sieved for 10 minutes through 63-micron filters to allow a homogenous distribution of spatial arrays to form.

Table 1. Methodology for composite powder synthesis

	Spatial Array	*Starting Ti-MMC*	*Ball-to-Powder Ratio*	*Mix Interval (on:off) [min]*
A	Ti-0.5BN	Ti-2.0BN	2:1	4:5
B	Ti-1.0BN	Ti-2.0BN	1:1	4:5
C	Ti-2.5BN	Ti-5.0BN	1:2	4:5

2. Processing Parameters for SLM

The additive manufacturing machine used for this thesis was the EOS M 100. This machine is compatible with three metal powders, cobalt-chrome, stainless steel 316L, and

Ti-64, each with specific software to optimize the print. The technical specifications are listed below by EOS:

- Building volume: 100 x 95 mm (3.9 x 3.7 in) (height incl. build plate)
- Laser type: Yb fibre; Laser 200 W
- Precision optics: F-theta lens; high-speed scanner
- Scanning speed: up to 7.0 m/s (23 ft./sec)
- Focus diameter: 40 µm
- Power supply: 200 - 240 V
- Power consumption max. 1.7 kW / average 0.60 kW

The manufacturers' setting to print Ti-64 results in an energy density of 60 J/mm^3. The settings were optimized for Ti-64 without any reinforcing particulates considered. As a result, to print the Ti-MMC, energy parameters were changed to achieve a dense, high-resolution part. All parts were created using an energy density of 25 J/mm^3. To obtain this energy density, the outer skin settings on the machine were also changed to the parameters listed in Table 2, to yield an energy density of 25 J/mm^3. These values were verified using Equation 1 from Chapter II Section C Part 1.

Table 2. Modified SLM energy density parameters

	Distance [mm]	*Speed [mm/s]*	*Power [W]*	*Thickness [m]*	*Energy Density [J/mm^3]*
Stripes	0.06	1400	42	0.02	25
Upskin	0.06	1400	42	0.02	25
Downskin	0.06	1120	33.6	0.02	25

The parts created were 10 mm and 20 mm squares, each of which was 3 mm in thickness a possessed 2 mm filleted corners. The orientation on the build plate was designed to eliminate the amount of contact each part had with the recoater blade. Insomuch, each part was oriented with a 15-degree offset from the blade, causing limited blade contact, if at all.

3. Heat Treatment of 3D Printed Composites and Control Sample

Half of the parts created were heat-treated to study how it affected the porosity. Heat treatment took place in a tube furnace with a constant argon flow at a tube pressure of ~0.4 MPa. After placing the parts in the furnace, the tube was vacuumed -0.04 MPa to remove the air. Inert argon gas was then purged to a pressure of 0.4 MPa, displacing any residual air. The pre-setup process was conducted five times before the vacuum was turned off, and the argon began to free flow at a pressure of ~0.4 MPa. This process was used to eliminate the potential of an oxide layer forming on the surface, causing the parts to corrode. The goal of this process was to reduce the porosity of the parts and eliminate any residual stresses. To do so, the furnace was heated from room temperature to 1000^{o}C in 90 minutes, held at 1000^{o}C for 90 minutes, and then allowed to cool in the furnace until room temperature.

4. Characterization of Composite Powder and 3D Printed Samples

Density measurements were carried out using an analytical balance configured for Archimedes principles measurements. Weights were taken of the 20 mm parts in the air and then submerged measurements were taken while the parts were placed in a basket suspended in water. After which, the air density and water density, based upon the temperature of each medium, were used to determine how dense each part was after fabrication.

After fabrication, the 10 mm samples were mounted in epoxy resin and then manually polished. Each sample was ground using 250, 600, 1200 grit paper and then polished using a 1-micron diamond suspended solution using time increments of at minimum 5, 10, 15, and 30 minutes, respectively. As the grinding and polishing progressed, the parts were rotated 90 degrees to verify uniform polishing and elimination of the

previous surface scratches. Half of the surface area of the parts were then etched for microstructure analysis using a scanning electron microscope. Using a modified Kroll's solution consisting of 10 ml HF, 4 ml HNO_3, and 85 ml H_2O, explicitly designed for etching titanium, each part was etched using intervals of 15 seconds to avoid damaging the parts. Verification of satisfactory surface conditions was carried out using an optical microscope to verify that the polishing and etched surfaces were effective.

Scanning electron microscope (SEM) imaging was used for both powder, and 3D printed part characterization. Using carbon epoxy paper, each of the powder samples was mounted, and a full spectrum of magnifications were used to characterize the mixed composite powders. Similarly, the cross-sectioned 10 mm etched parts were mounted using copper and carbon epoxy for electron conduction. After which, the SEM was used to identify the microstructures and wear mechanisms present in the SLM parts using various magnifications.

B. POWDER ANALYSIS

1. Ti-1.0CeO_2

When CeO_2 was mixed with Ti-64, the titanium maintained its spherical shape while the CeO_2 adhered to the Ti-64 spheres, as shown in Figures 5–7. Adequate dispersion was present while it appears very few CeO_2 particles were free-standing, based upon the appearance of the carbon tape below. However, agglomerates of undispersed CeO_2 particles caused undesirable fusion between particulates shown in Figure 6. Although the intended powder characteristics were met, this powder was not analyzed any further.

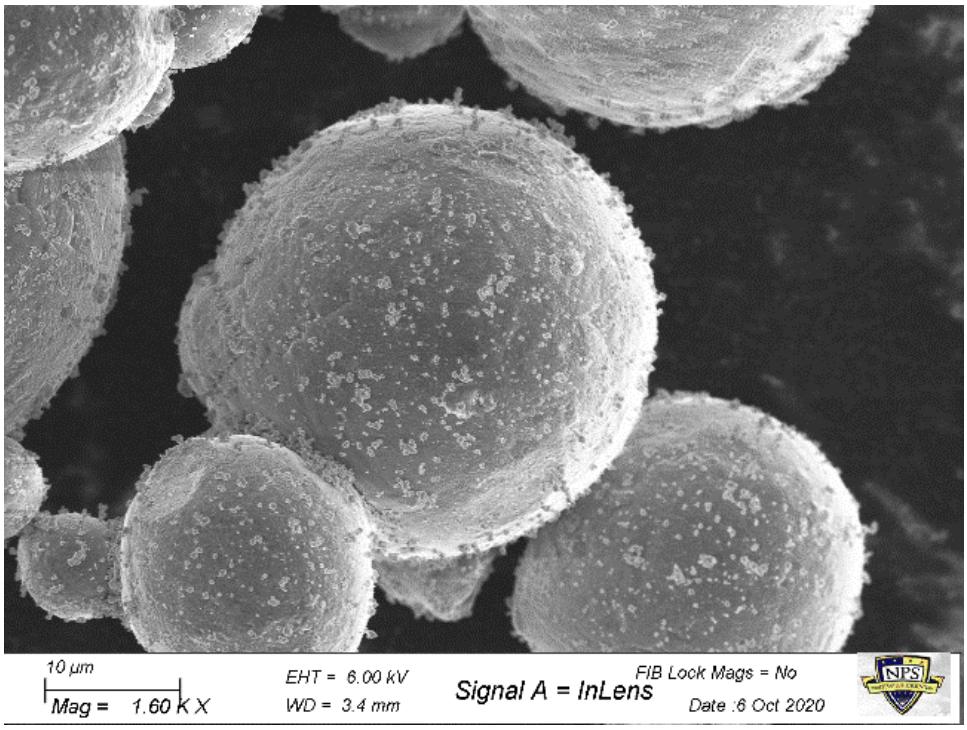

Figure 5. High magnification image of Ti-64 with CeO_2 reinforcement

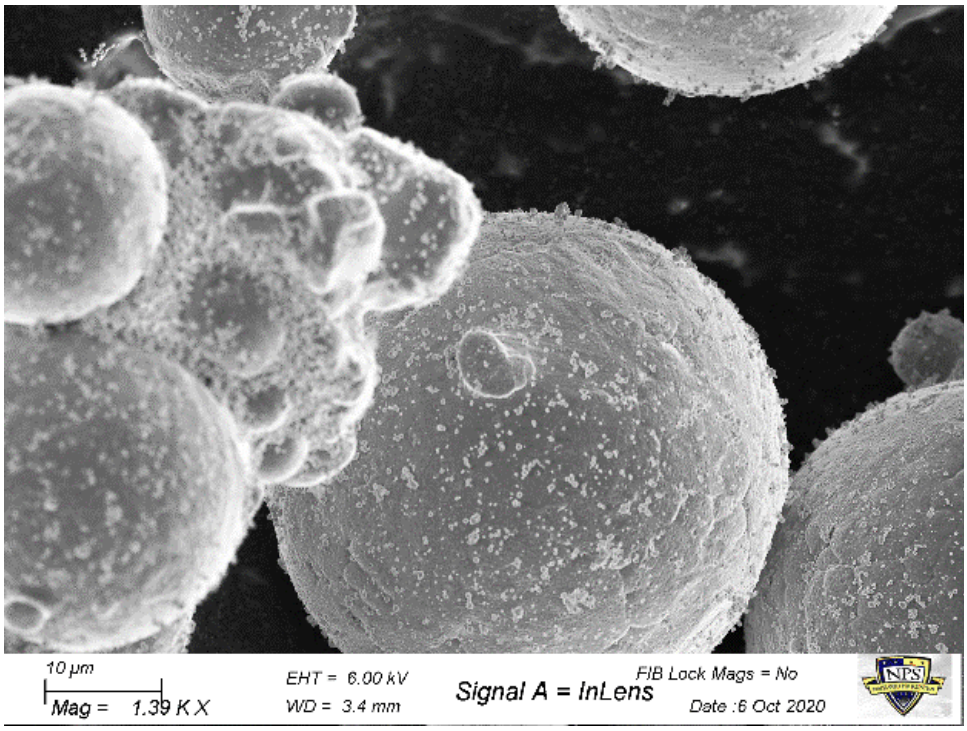

Figure 6. Ti-1.0CeO_2 SEM image showing particle fusion

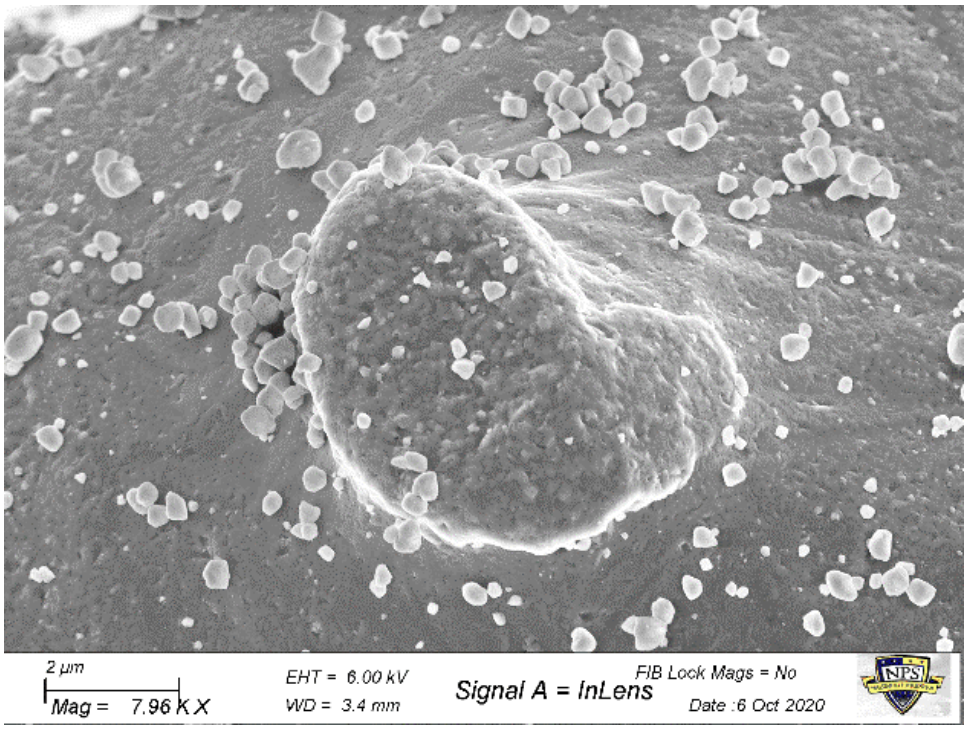

Figure 7. High magnification SEM image of Ti-64 surface showing signs of distortion and CeO_2 agglomerates forming

2. Ti-0.5 BN Spatial Array

The starting matrix shown below in Figures 8–10 corresponds to powder A from Table 1, which was used to create the Ti-0.5BN spatial array. This powder exhibited a reduction in spherical geometry compared to the Ti-CeO_2; however, it showed a significant reduction in the number of fused particles in the matrix. This can be attributed to the HEBM configuration changes resulting in plastic deformation caused by an increase in ball ratio and mixing intervals. Despite the loss of the shape, the BNNP adhered to the surface well, as shown in Figures 8–10, showing clean carbon paper indicative of a small amount of freely suspended BN particulates. Multiple BNNP are shown to have kept their platelet structure while cohered to the surface of the Ti-64. Figures 9 and 10 show a BNNP that appears to be embedded in the surface of a Ti-64 particle, covered by other BNNP residue, and another BNNP gently adhered to the surface.

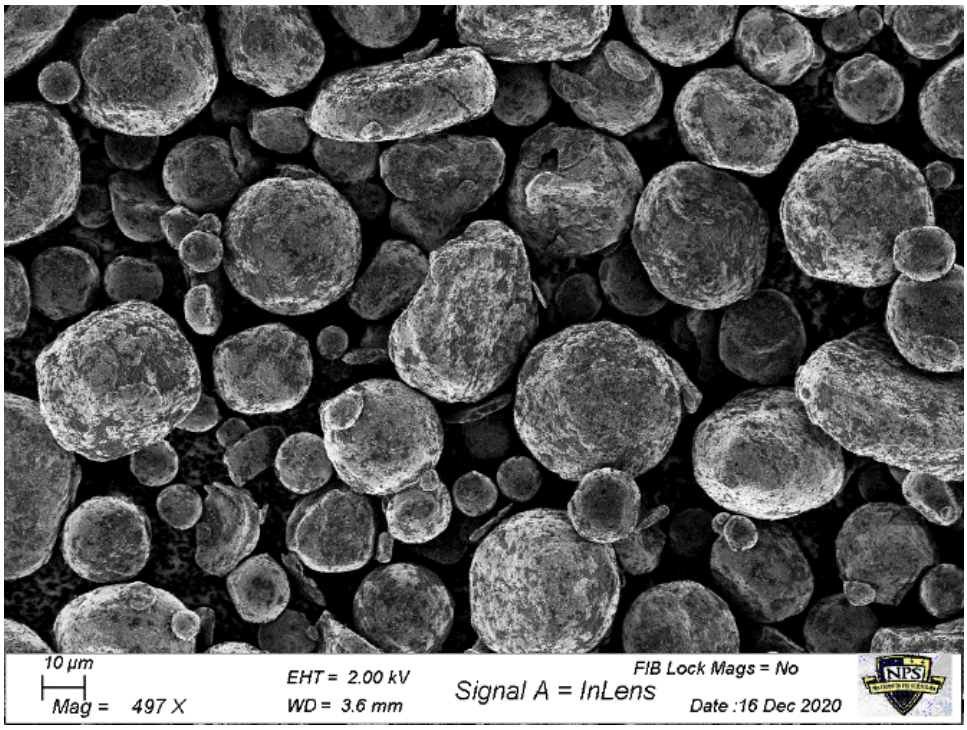

Figure 8. Low magnification SEM image of Ti-2.0BN (Powder A) showing particulate losing their spherical shape

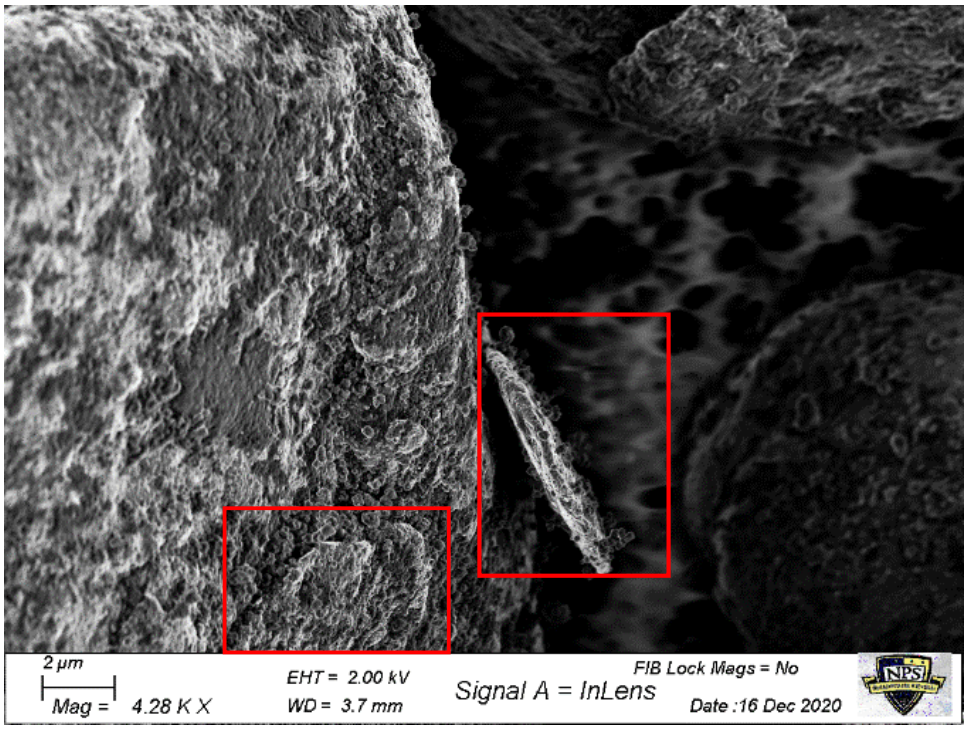

Figure 9. SEM image of Powder A showing BNNP imbedded in (left) and suspended from (right) the surface of a Ti-64 particle

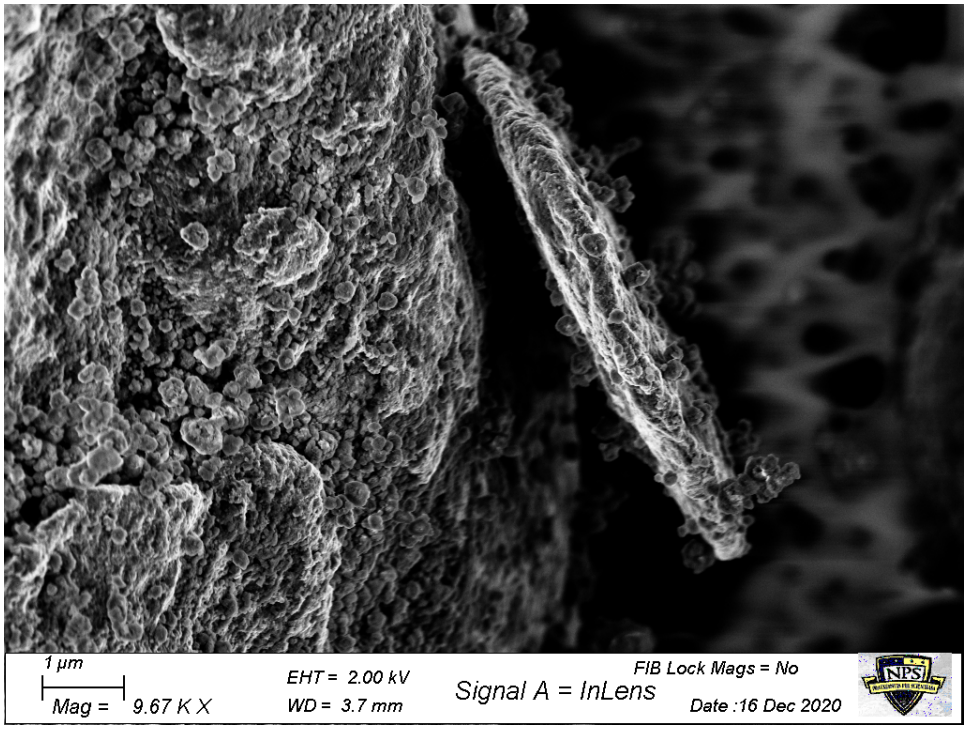

Figure 10. High Magnification SEM image of Powder A showing a BNNP

3. Ti-1.0 BN Spatial Array

The composite powder used to create Ti-1.0BN, powder B from Table 1, spatial array maintained its spherical shape at the dispense of causing more agglomerates. Using a lower ball ratio for mixing resulted in less plastic deformation of the Ti-64 particles but allowed particle fusion. As a result, the composite powered was re-sieved through the 63-micron filter to remove the large agglomerates before forming the spatial arrays. Despite the increased agglomeration, this powder showed adequate dispersion and platelets that maintained their shape through the HEBM process. The characteristics of these powders are more beneficial for the SLM process since they promote a more effortless flowability and more densely packed layers. Figures 11–13 show powder B at various magnifications with emphasis on the identification of platelets.

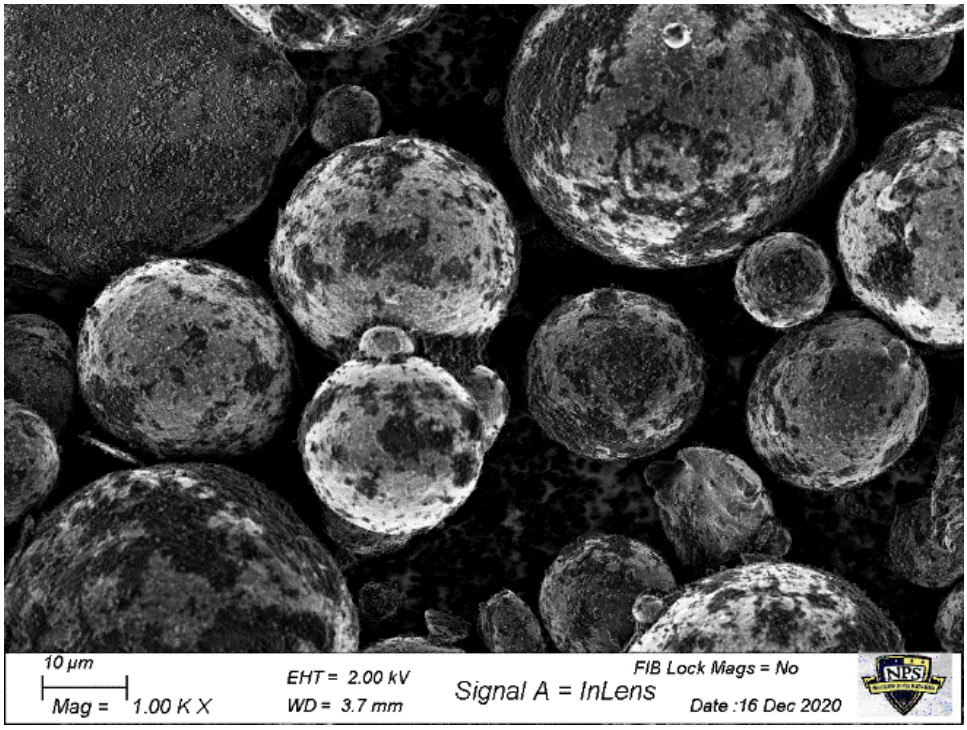

Figure 11. Low Magnification SEM image of Ti-2.0BN (Powder B)

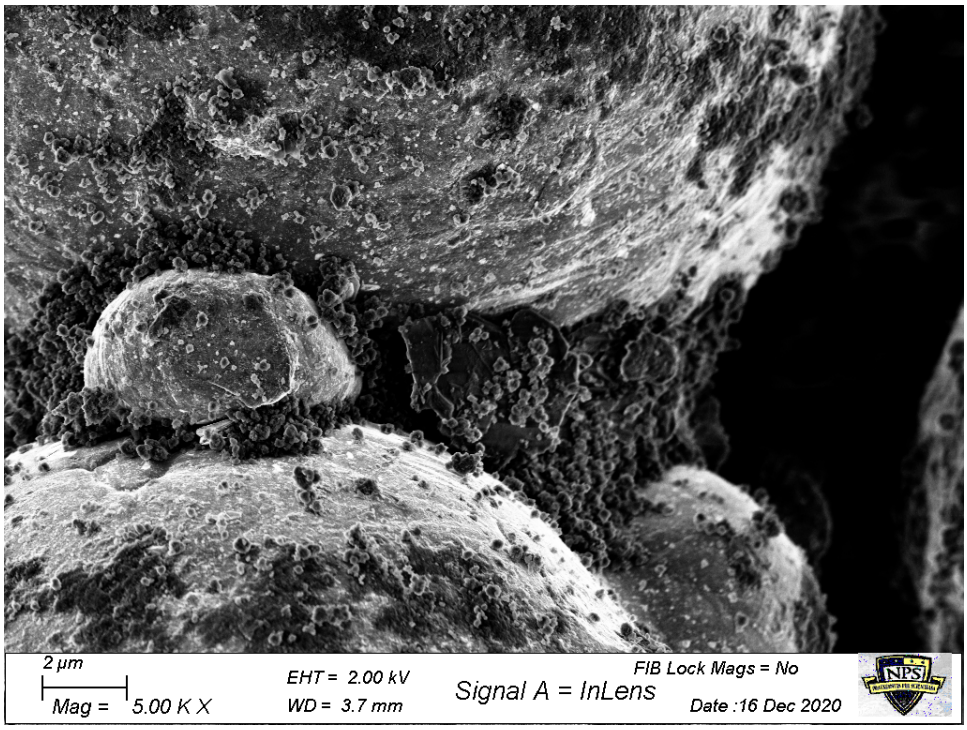

Figure 12. SEM image of Powder B showing particle fusion

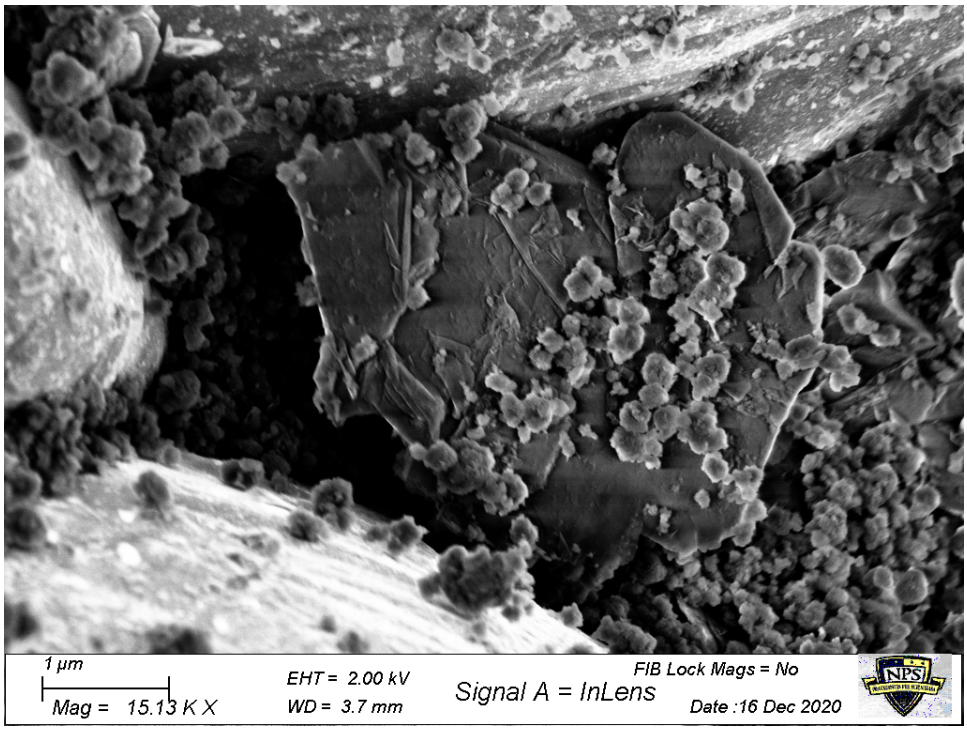

Figure 13. High Magnification SEM image of Powder B showing a BNNP

4. Ti-2.5 BN Spatial Array

The Ti-2.5BN composite spatial array was formed using a more significant BNNP volume percent composition than all the other samples. Figures 14–16 highlight the increase in platelets able to be maintained through the ball milling process. Using 5-volume percent instead of a 2-volume percent, the composite powder yielded from powder C in Table 1 showed the same spherical structure, but the carbon paper is covered by BNNP particulates that did not attach to the Ti-64 surface. Since the volume percentage doubled for powder C, the amount of freely suspended particulates was expected. Considering the increase in the number of platelets maintained, this powder was expected to exhibit the most drastic changes when manufactured using SLM.

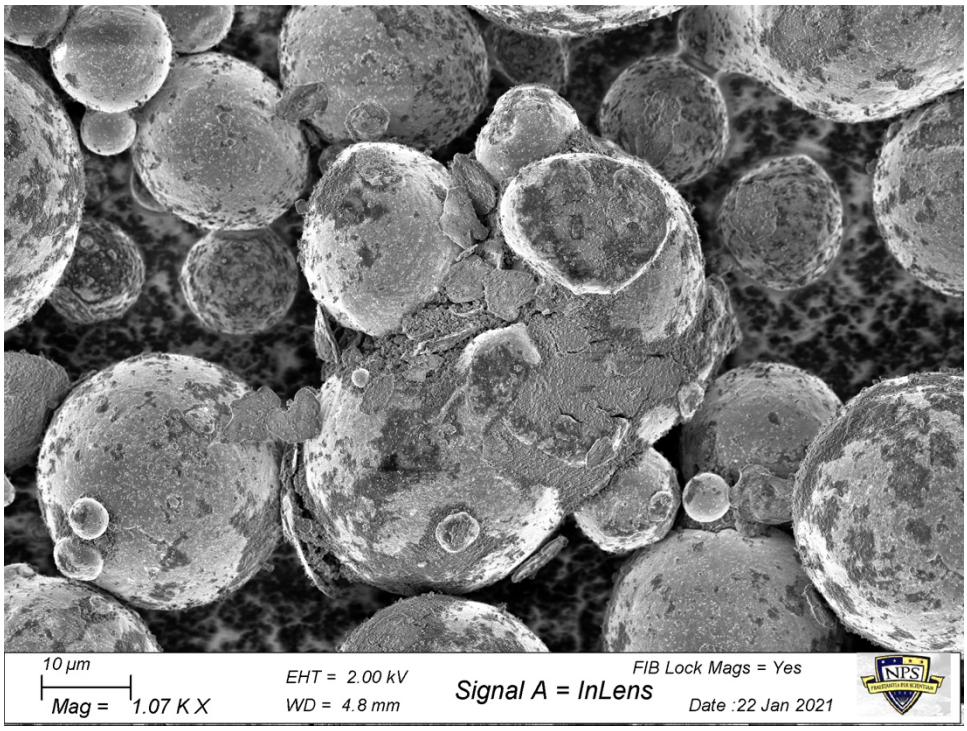

Figure 14. SEM image of Powder C

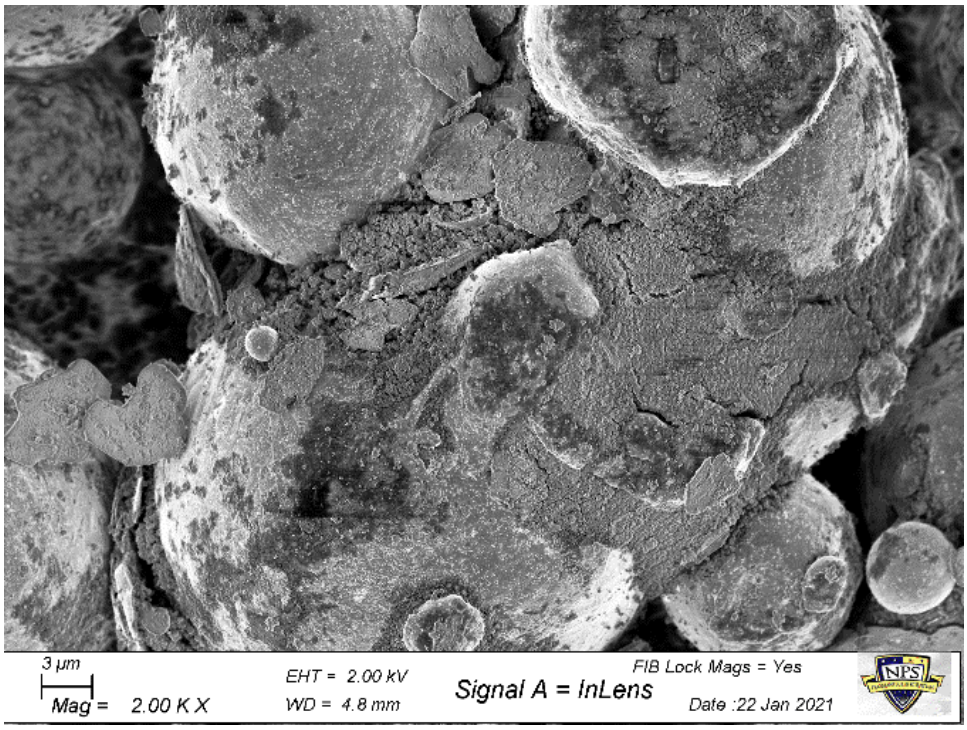

Figure 15. SEM image of Powder C showing an abundance of full BNNP

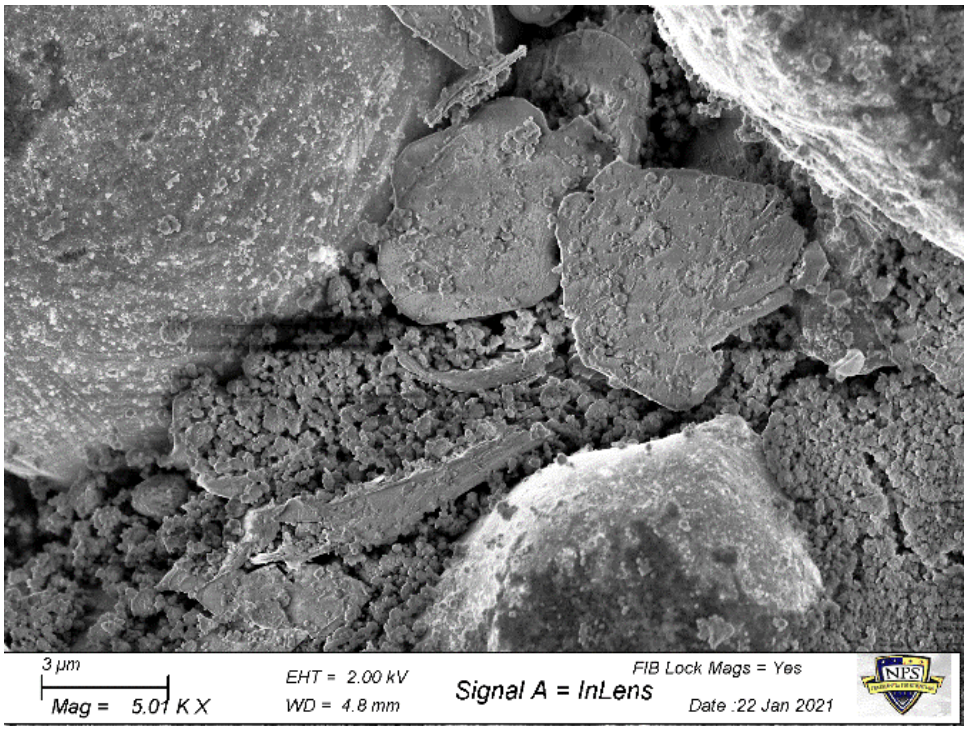

Figure 16. High Magnification SEM image of Powder C showing many platelets collecting between Ti-64 particles

C. DENSITY AND MICROSTRUCTURE OF SLM PARTS AS PRINTED AND HEAT TREATED

1. Relative Density

The fabricated samples' relative densities were compared based upon the volume percentage of reinforcement. Heat treatment increased the densification of all parts except for the Ti-2.5BN composite, but the Ti-64 sample benefited the most from the post-processing. This can be attributed to a reduced amount of diffusion as the amount of BNNP increased. Since the as-printed Ti-2.5BN part had close to 98% relative density, the BNNP were likely unable to diffuse despite the high temperature, leaving behind large pores. Figure 17 shows that the Ti-2.5BN composite is very porous, contradicting the results of the Archimedes density measurement.

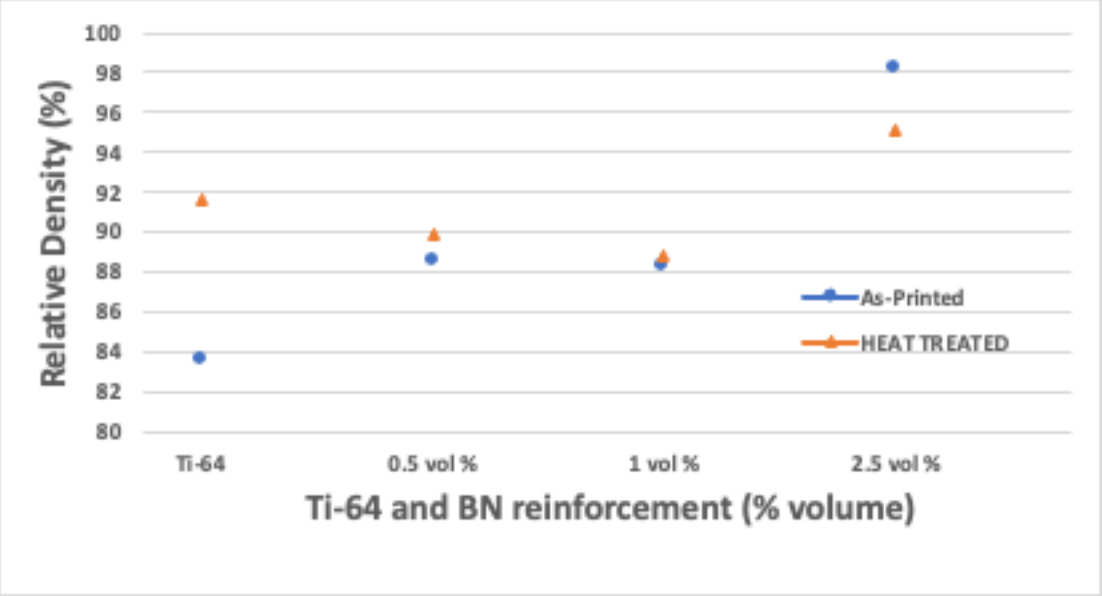

Figure 17. Relative Density of Printed Samples Measured Using Archimedes Principle

To verify the densities calculated using Archimedes principle were factual, the OM and IMAGEJ was used to confirm the results. Using a binary, 8-bit, gray scaled image, IMAGEJ was able to discern between the porous and metallic areas on the surface of the polished samples. Assuming the pores are uniformly distributed throughout the sample, an

accurate calculation of the density can be performed. As can be seen in Figure 18, the Archimedes principle method was very erroneous when used with a porous sample and provides conflicting results. It is apparent that the heat treatment method was only successful when using very low volume percentages of BNNP. The heat-treatment method used was designed for Ti-64 evident based upon Ti-64 increasing in density to 93% dense.

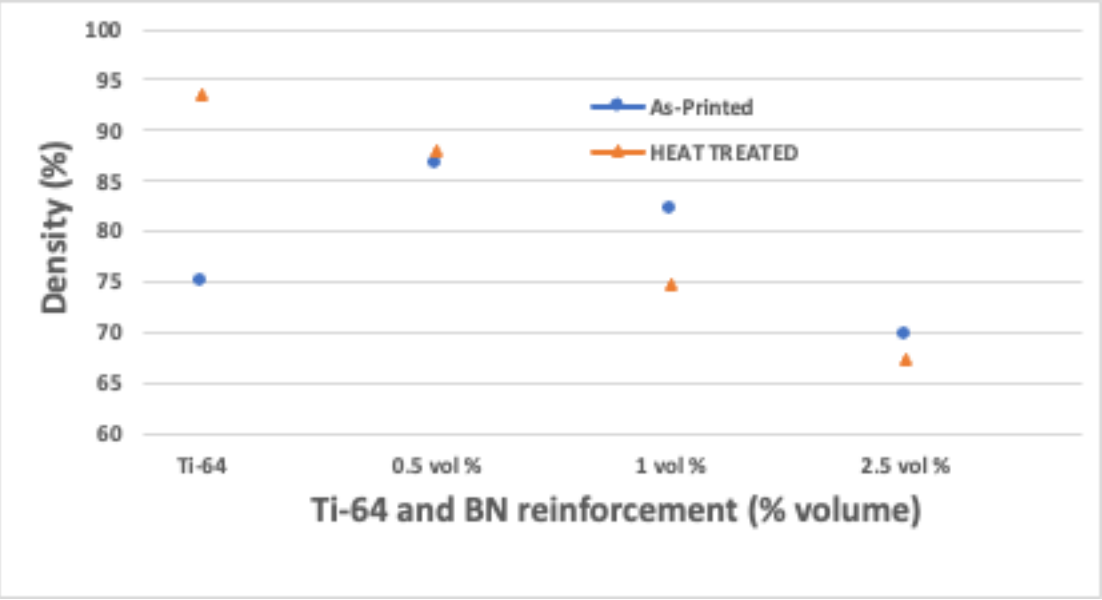

Figure 18. Density Measured Using ImageJ

2. Microstructure

Microstructure identification took place in the SEM. The changes were evaluated by comparing the as-printed Ti-64 sample's microstructure to the as-printed Ti-2.5BN sample. The modified Kroll's etchant revealed the α + ß phases typical of Ti-64. Figure 19 shows a large amount of ß phase indicated by dark gray, lighter needle-like structures coinciding with the α phase, and the faint, white, uniformly dispersed particles most likely represent α'. The larger agglomerates can be disregarded, as they are suspended on the surface because of the mounting process. Noticeably, the dark ß phase dominates the SLM part, with α phase uniformly distributed throughout with various lamellar thicknesses. Regarding the α' phase, Figure 20 shows a region which appears to have α' imbedded in the surface.

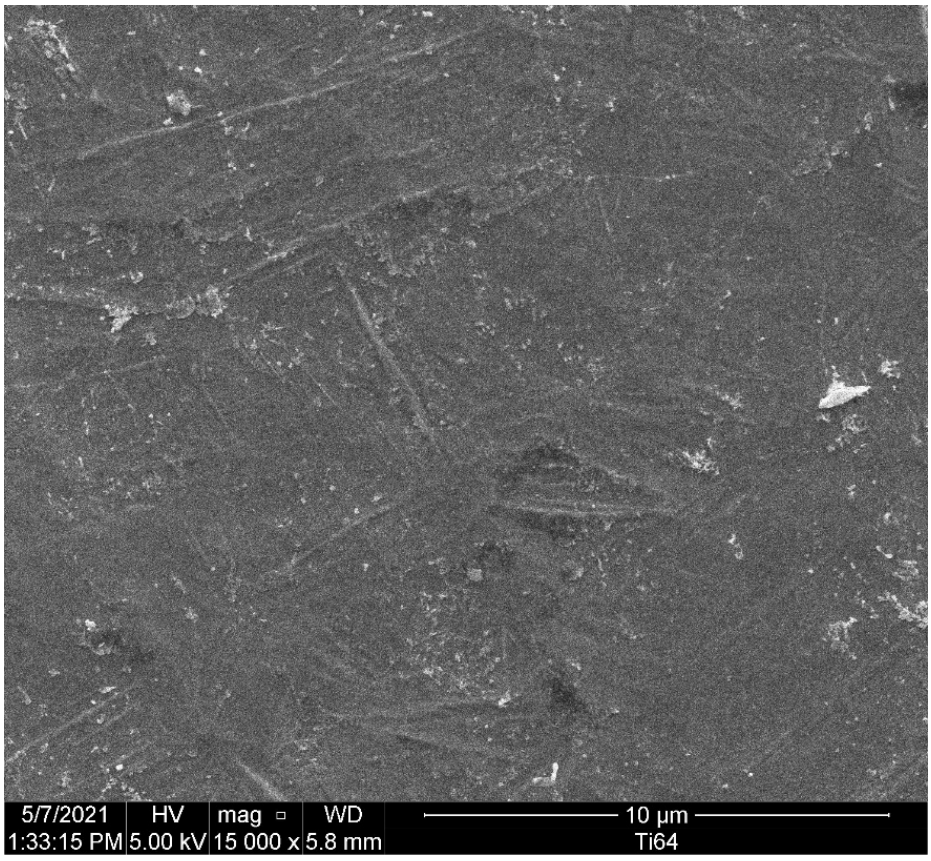

Figure 19. SLM Ti-64 sample showing uniform lamellar microstructures

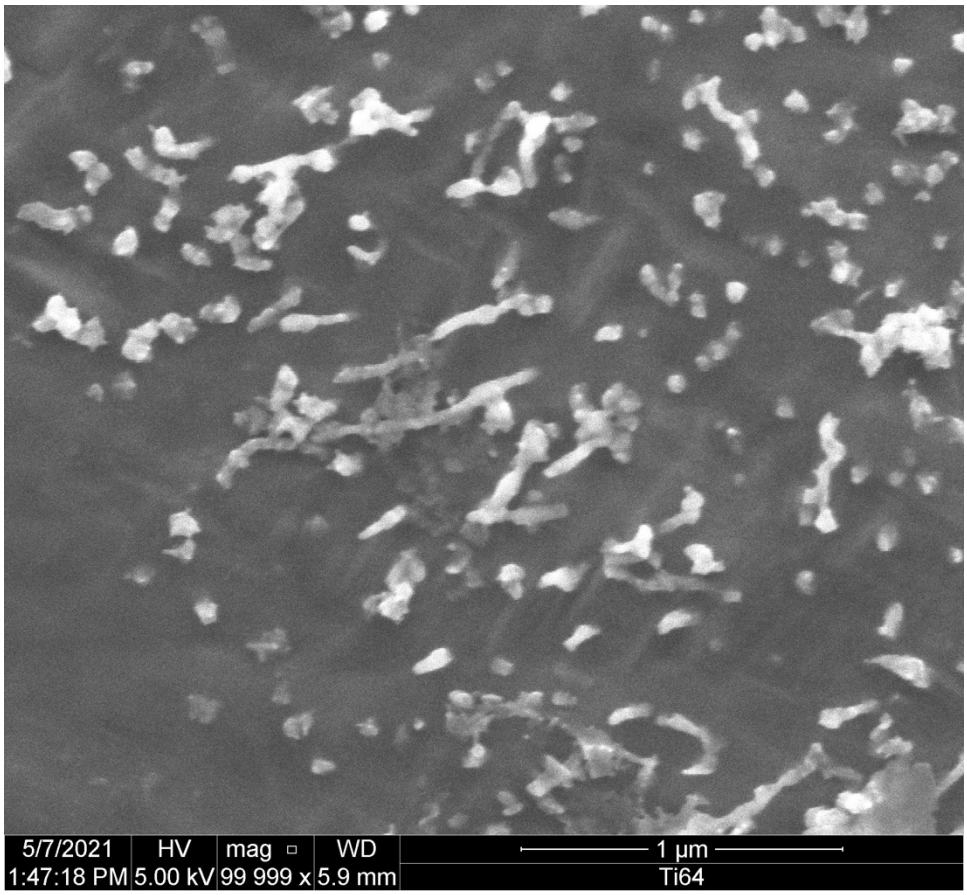

Figure 20. SLM Ti-64 sample with indications of α’ precipitate

As the composition of BNNP increased, the microstructure stayed relatively consistent. Figure 21 shows the microstructure formation of Ti-2.5BN, which appears to have precipitated a larger quantity of α’ that was uniformly dispersed throughout the sample. Contrarily, a noticeable reduction in the amount of needle-like α lamellas is evident. He et al. [39] also experienced the same transformation when SLM was used to contribute to the rapid heating causing α’ to form and the quick cooling which does not allow for the α phase to proliferate. Just as in the Ti-64 sample, the ß phase dominates the sample but the increase in α’ is beneficial to increasing the hardness. Unfortunately, the BNNP were unable to be identified within the sample using the SEM.

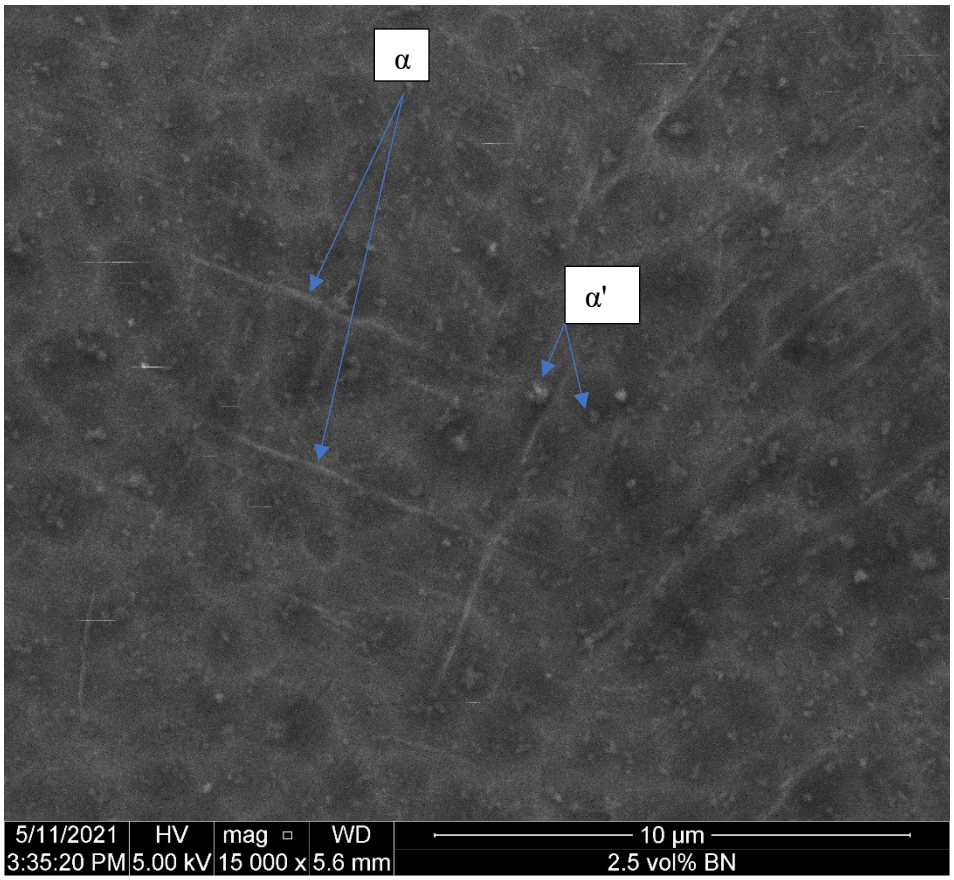

Figure 21. SEM image of printed Ti-2.5BN sample showing α' and α phases

Another critical insight regarding the Ti-2.5BN sample is how reducing the energy density caused unmelted particles to form. Figure 22, a low magnification image of the Ti-2.5BNs surface, shows many unmelted particles mostly oriented along the edge of pores. This formation of these pores is directly related to decreased energy density causing a lack of fusion between particles [38].

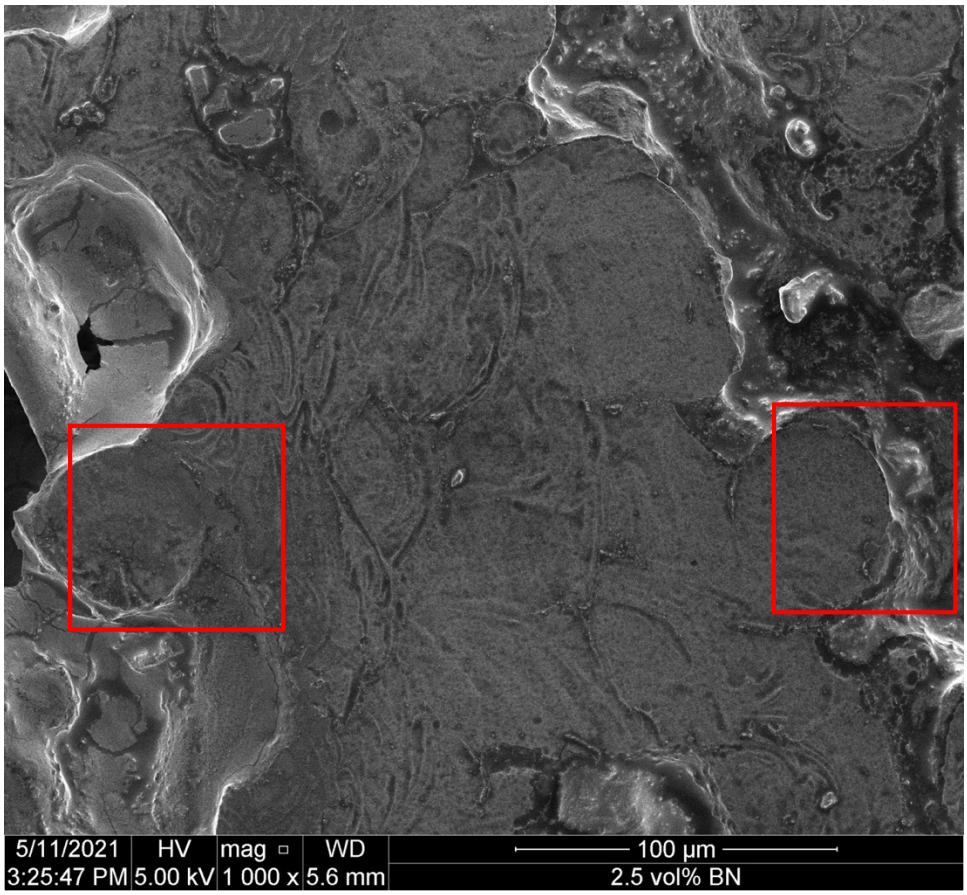

Figure 22. Low Magnification SEM image highlighting unmelted particles on the surface of the Ti-2.5BN SLM sample

THIS PAGE INTENTIONALLY LEFT BLANK

IV. MECHANICAL PROPERTIES

A. MATERIAL HARDNESS AND WEAR RESISTANCE CHARACTERIZATION METHODS

1. Hardness Testing

Microhardness testing was carried out in a Struers Durascan 50 Vickers hardness tester. Each sample was polished using the specifications listed in Chapter III Part A Section 4 to remove the epoxy, obtain a uniform polish, and remove scratches. Surface scratches, which act as cold working and pores, can skew the localized hardness values. Using an HV of 0.5, the Vickers microhardness diamond-shaped indenter was forced under constant pressure into the surface of each sample, and the edge distances were measured to assess the depth of the indentation. Smaller depth equates to harder material; the opposite is true of softer materials, which penetrate deeper into the material. For each part, a minimum of 10 measurements was taken to confirm uniform localized hardness throughout the build.

2. Wear Testing

Tribological properties were measured using the Nanovea T50 tribometer. This machine can perform rotational, linear, and block-on-ring wear testing. The SLM parts were mounted to a rotating disc that performed dry sliding against a 3 mm alumina ball that acted as the abrasive material. Alumina was used because of its immense hardness that can withstand the duration without significant wear. Doing so allowed for the coefficients of friction (COF) and wear resistance to be examined as a function of the normal force and wear track depth. Each test used the following parameters:

- Normal Force: 5 N
- RPM: 200 RPM
- Radius: 2 mm
- Time: 30 minutes

The linear variable differential transform (LVDT), which measures linear motion and converts it into electrical signals, was graphed as a function of wear distance. This data was then inverted and normalized to show the trend of wear resistance as the distance increased. In terms of the contact force, the Hertzian contact stress calculation was used to estimate the amount of contact force applied to the plates via the 3 mm diameter ceramic balls. Assuming a Poisson's ratios of 0.21 and 0.31, elastic moduli of 370 and 110 GPa for alumina and Ti-64, respectively, and a normal force of 5 N, it resulted in a max contact pressure of 1544.8 MPa.

B. HARDNESS BEHAVIOR

Hardness was influence by the addition of BNNP, as shown by the averages in Table 3 and Figure 23, the as-printed samples steadily increased as the Ti-MMC increased the volume percentage of ceramic reinforcements. A 36% hardness increase from the control Ti-64 sample. This trend correlates to what should be expected based on other papers that tested ceramic reinforced Ti-MMC [21,33]. The large standard deviation values of each material are reflective of defects like pores.

Heat treating the parts decreased the hardness in each sample. The Ti-0.5BN matrix experienced the most unique change, as it was the only Ti-MMC that increased in hardness but within one standard deviation, albeit. Thermal stresses could cause this phenomenon because all of the lower ceramic reinforcement compared to Ti-64 [31]. Ceramics, by nature, have low thermal conductivity and high elastic moduli and because the parts were slowly cooled this could have affected the hardness. The manufacturer recommends heat treatments being performed on the standard printed Ti-64 parts at 800ºC; however, as indicated in Chapter III Part A Section 4, each of the parts were sintered at 1000ºC. The residual stresses that form because of the SLM process, could have caused the increase in hardness. Likewise, the stresses could have been relieved post-heat treatment due to a hysteresis loop that resulted in a more ductile part once it was exposed to heat [39]. Additionally, phase changes will occur when heated to 1000ºC, for 90 minutes. the could have resulted in a reduction or total loss of the martensitic α' phase since it decomposes at around 650ºC [37,38]. Alternatively, that more ß phase is present because of being slowly

cooled in the furnace from above the α+ß transformation point since the α phase is harder by comparison [46].

Table 3. Tabulated hardness and standard deviations of each Ti-BN composition

As-printed		
Composition (Vol %)	Average (GPa)	STD DEV (GPa)
Ti-64	3.68	0.55
0.5	3.00	0.36
1.0	4.32	0.40
2.5	5.00	0.47
Heat Treated		
Ti-64	2.84	0.55
0.5	3.54	0.52
1.0	4.29	0.30
2.5	4.74	0.11

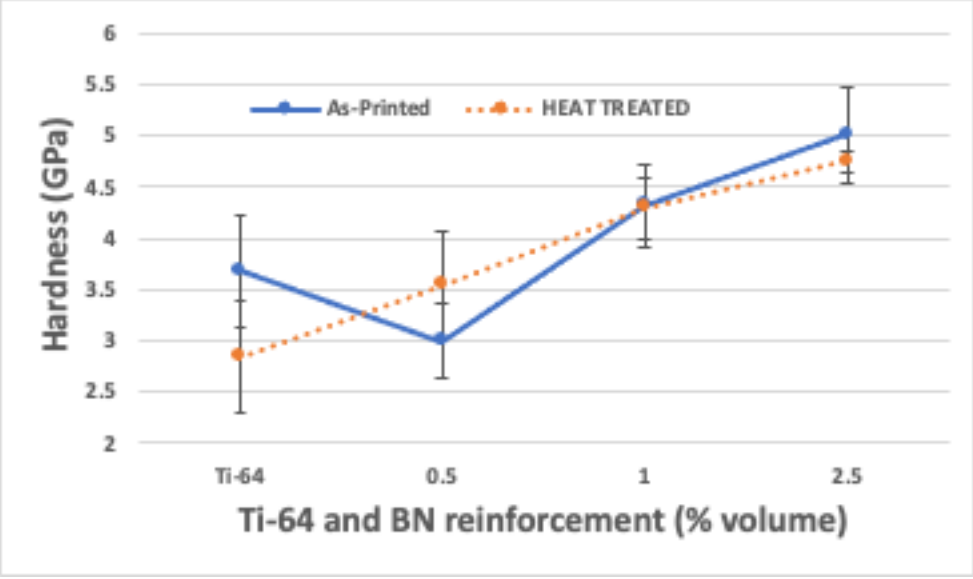

Figure 23. Microhardness vs Ti-64 and BN reinforcement (% Volume)

C. WEAR PERFORMANCE

1. As-Printed

Wear behavior was evaluated using a dry sliding wear method. As can be seen in Figure 26, the COFs for each sample were relatively close in value. However, as the volume percentage of BNNP increased the average COF also increased, where 0.48, 0.52, 0.57 correspond to 0.5, 1.0 and 2.5 volume percentages, respectively. All of which were lower than the pure Ti-64 sample which has an average COF of 0.59. Figure 26 shows the COF plotted vs distance which is represented by a 50-point average to reduce the amount of noise in the system. The raw data of each sample was refined using the same parameters and Nanovea's proprietary software to maintain consistency. From inspection, it appears that each samples COF increased linearly for approximately 13 m, indicating there was a wear-in period which increased in conjunction with the increasing amount of surface area that contacted the ceramic ball [47]. The COF of Ti-0.5BN, appeared to be decreasing in value as the distance increased, reaching its maximum COF directly as the wear-in period ended and subtly decreasing to its minimum value as the testing terminated. Ti-64, Ti-1.0BN and Ti-2.5BN remained constant after the wear-in period.

Figure 24 shows an SEM image of a portion of the as-printed Ti-2.5BN wear track. At low magnification it is apparent pores exist throughout the wear track which act as collection points for residue which acts as third-body abrasion. This type of wear is detrimental to the wear resistance because as the wear depth increases the ceramic particulates become exposed hastening the wear process [21]. Despite the many pores, high magnification SEM images reveal the Ti-2.5BN part exhibiting signs of adhesive wear and visible BNNP. This type of wear is a result of the Ti-MMC being softer than the alumina balls and is the preferred mechanism since it is results in a smooth surface [47]. Amanov et al. [47] experienced the same adhesive wearing when performing dry slide testing SLM Ti-64 parts against a SAE-52100 steel ball bearing. Additionally, Figure 25 highlights regions which appear to be BNNP based upon their electron transparency and apparent contrast.

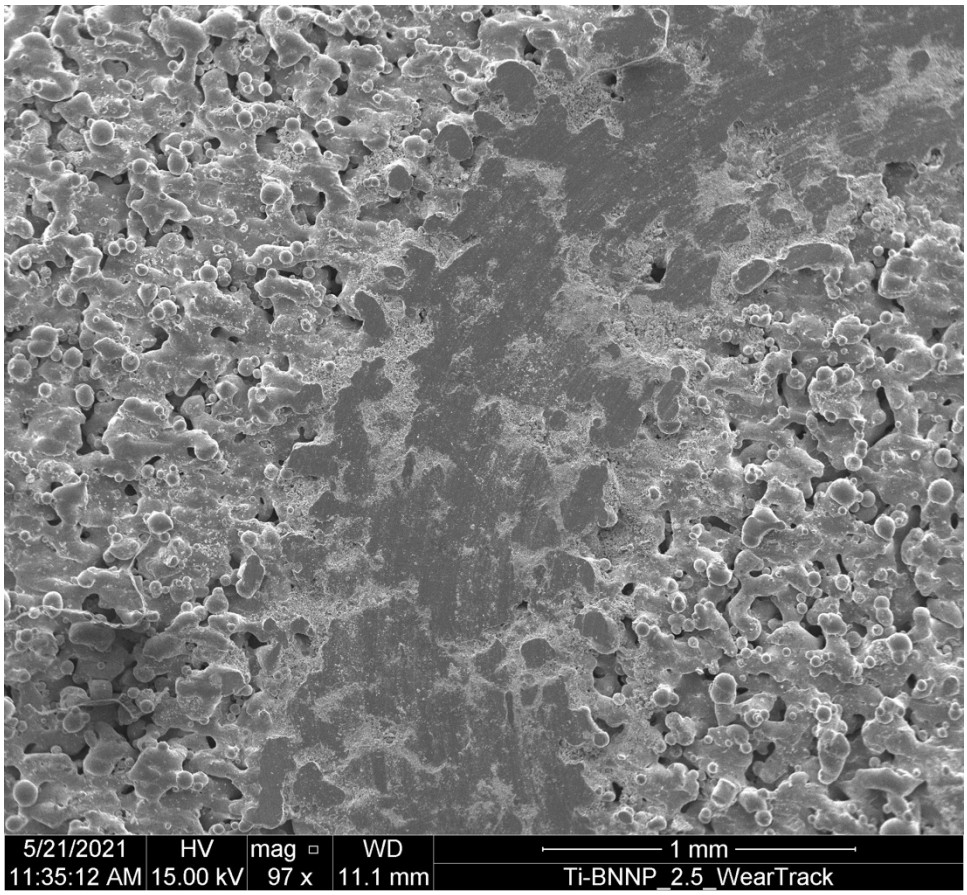

Figure 24. Low Magnification SEM image of Ti-2.5BN as-printed wear track showing pores filled with wear debris

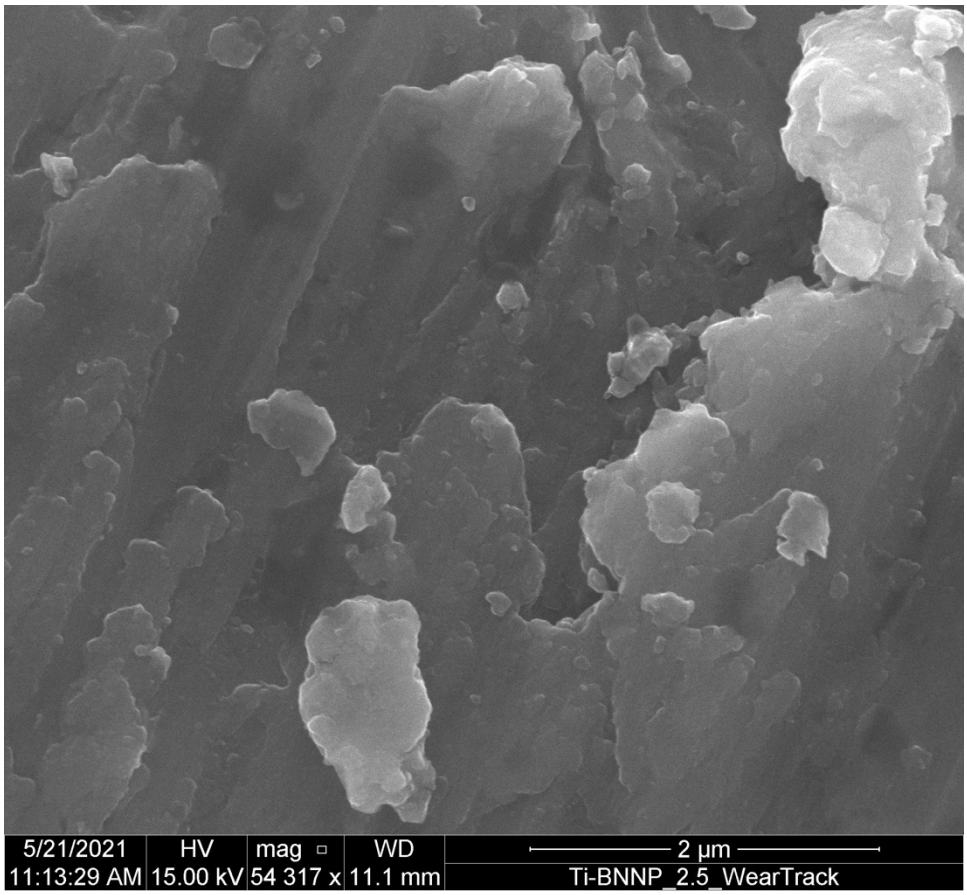

Figure 25. High Magnification SEM image of Ti-2.5BN as-printed wear track indicating adhesive wear and intact BNNP

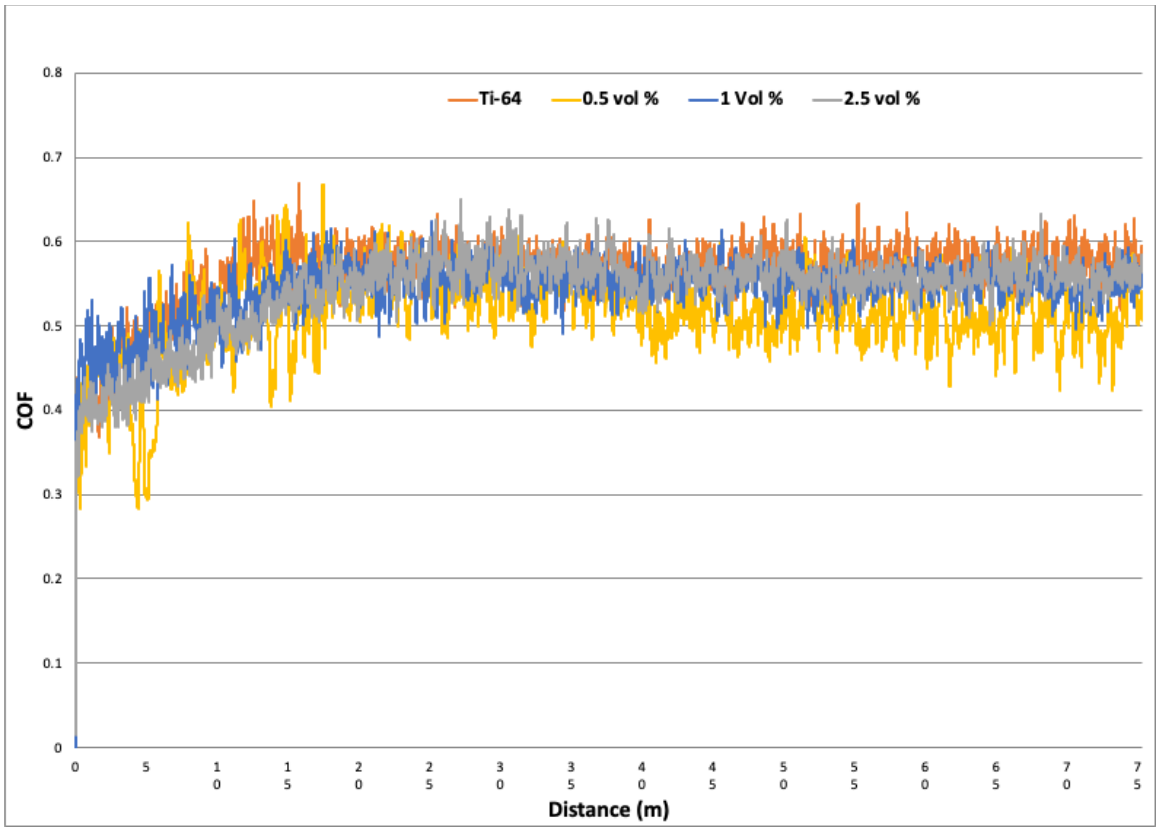

Figure 26. As-printed COF vs Distance

Depth measurements were also graphed as an indication of wear resistance. As shown in Figure 27, BNNP reinforcements caused an increase in the wear depth. This is attributed to the increased porosity that the Ti-MMC parts possessed because of lower energy density. Initially the Ti-0.5BN composite followed a similar depth profile as the Ti-2.5BN but slowly decreased with time. Of note, wear rates appear to be decreasing upon termination of the wear-in period but Ti-0.5BN experiences the largest decrease in wear rate. Overall, Ti-0.5BN displayed superior enhancements in wear resistance in the as-printed parts unlike the Ti-1.0BN and Ti-2.5BN composites.

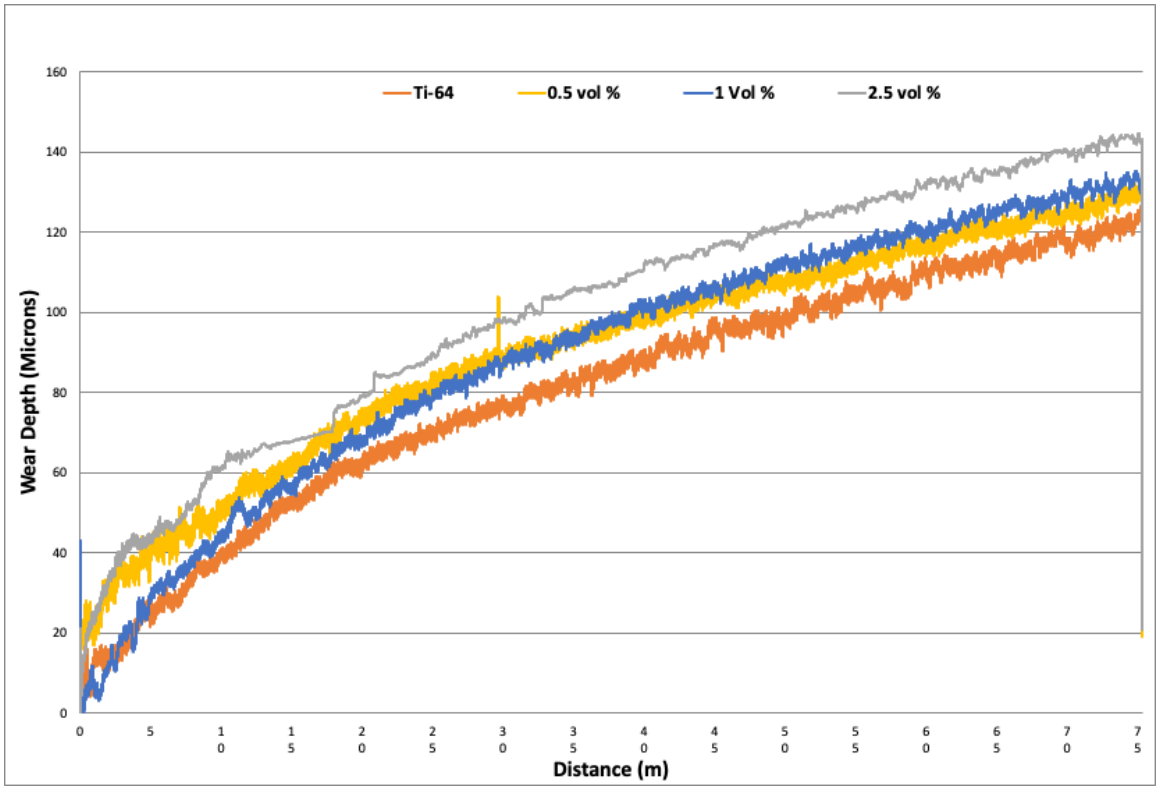

Figure 27. As-printed Wear Depth vs Distance

2. Heat Treatment

The heat-treated parts followed a different trend entirely. For starters Ti-64 which averaged a COF of 0.57, no longer possessed the highest COF instead its COF was reduced by 30%. Regarding the other samples, their COF were 0.48, 0.62, 0.70 for Ti-0.5BN, Ti-1.0BN and Ti-2.5BN, respectively, all of which are indicated in Figure 28. The Ti-64 samples wear resistance benefited the most from the heat-treatment opposite of what was expected based on hardness values. Although the composites all possessed superior hardness values after being heat treated, the composites show higher COF after heat treatment.

The wear depth data for the heat-treated samples has very obfuscated results shown in Figure 29. Assuming porosity played a major role in the high COF for Ti-1.0BN and Ti-2.5BN and their ability to resist wear depth correlates to their superior hardness. Not only do pores collect debris, they also represent stress concentration areas that can reduce the

mechanically properties when dynamic loading is applied [38]. Despite Ti-1.0BN and Ti-2.5BNs increased porosity they were still capable of producing very similar wear depths to the Ti-64 sample.

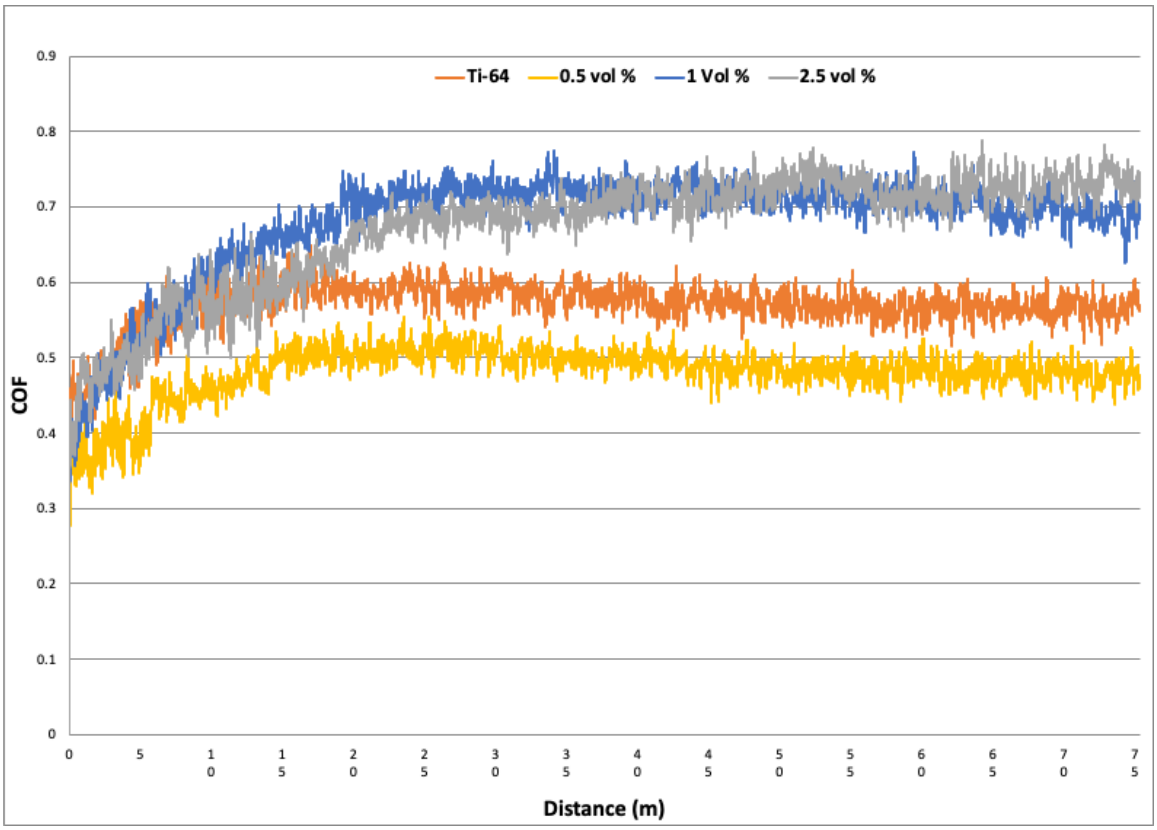

Figure 28. Heat Treated COF vs Distance

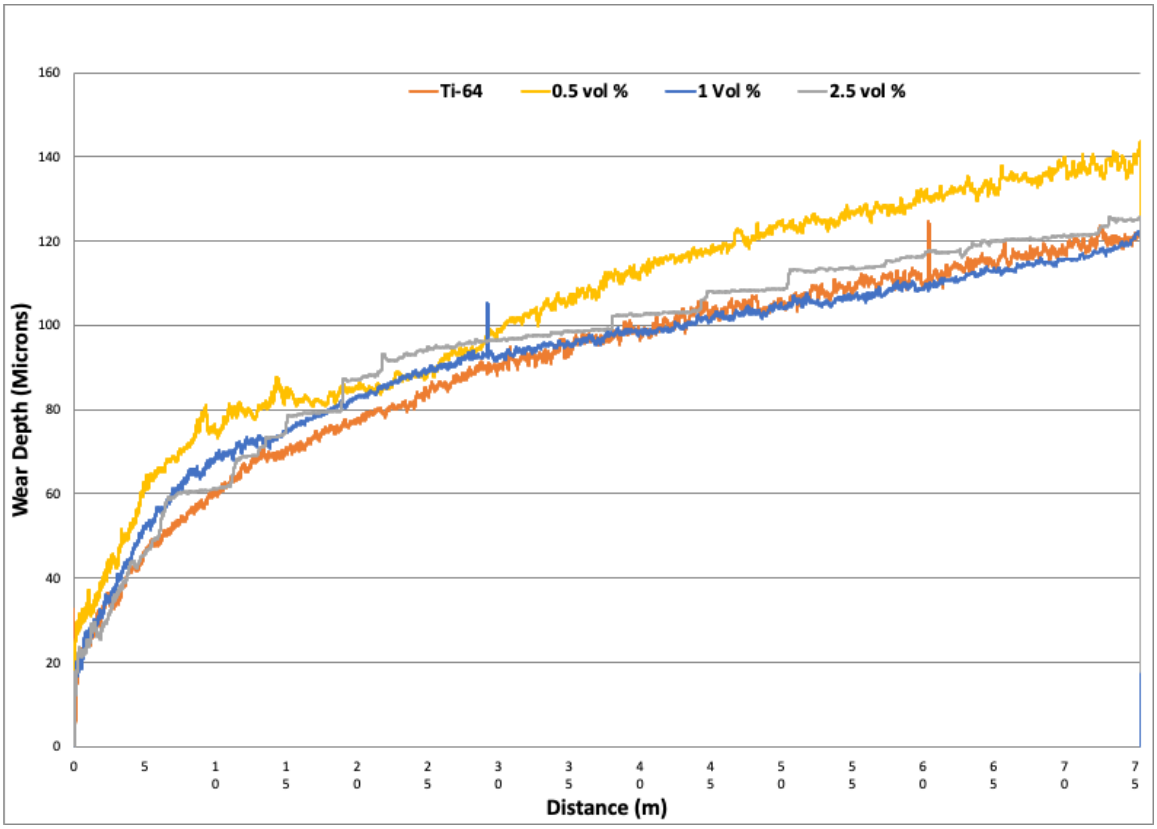

Figure 29. Graph representing wear depths for heat treated samples

After heat treatment the Ti-2.5BN showed a reduction in the amount of pores that were present within the wear track. Reduction in pores equates to less areas for debris deposition which is beneficial to mitigate the effects of third-body abrasion. Figure 30 shows smooth wear tracks with pores dispersed throughout. Using higher magnification SEM images like Figure 31, unmelted particles were revealed, and the same adhesive wear profiles experienced by the as-printed Ti-2.5BN sample were present.

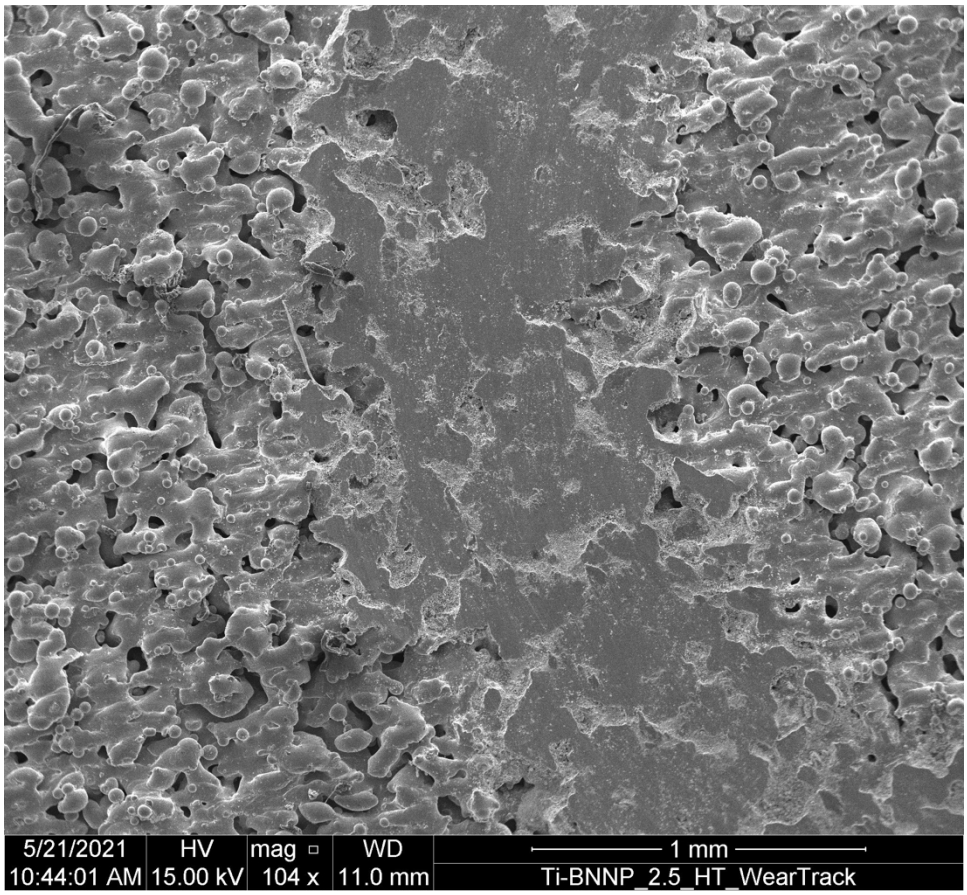

Figure 30. Low Magnification SEM image of Ti-2.5BN heat treated wear track

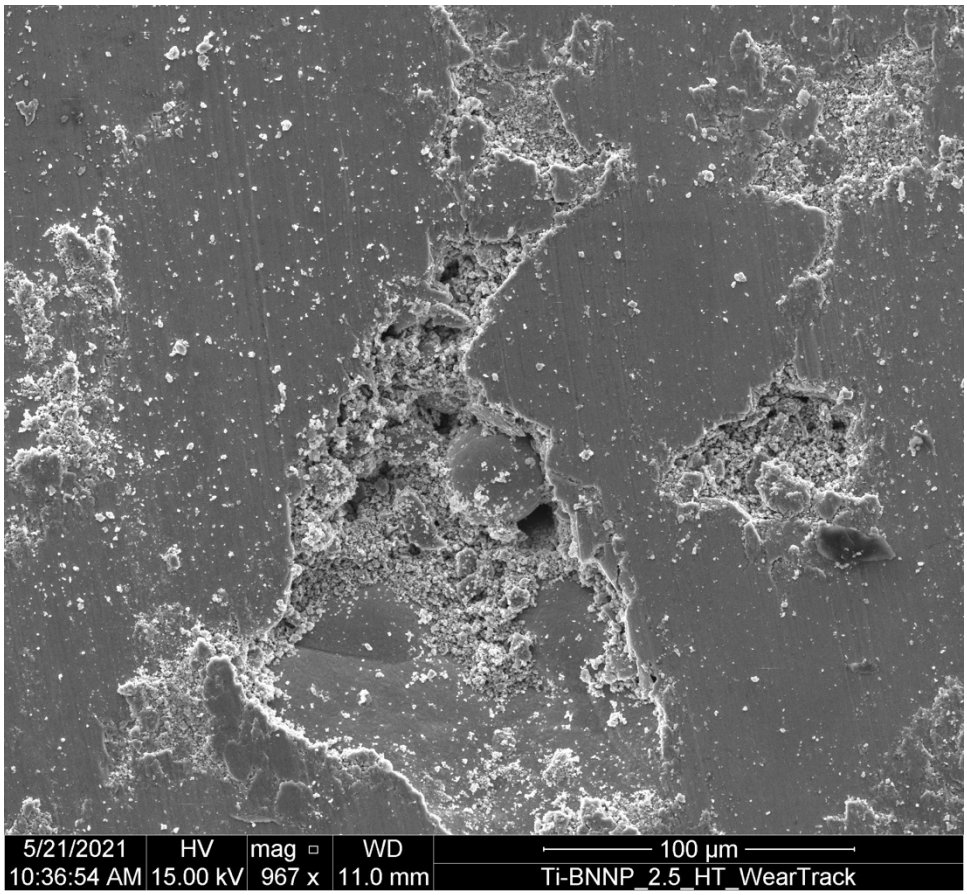

Figure 31. Medium magnification image of Ti-2.5BN heat treated part showing wear debris, an unmelted particle and adhesive wearing

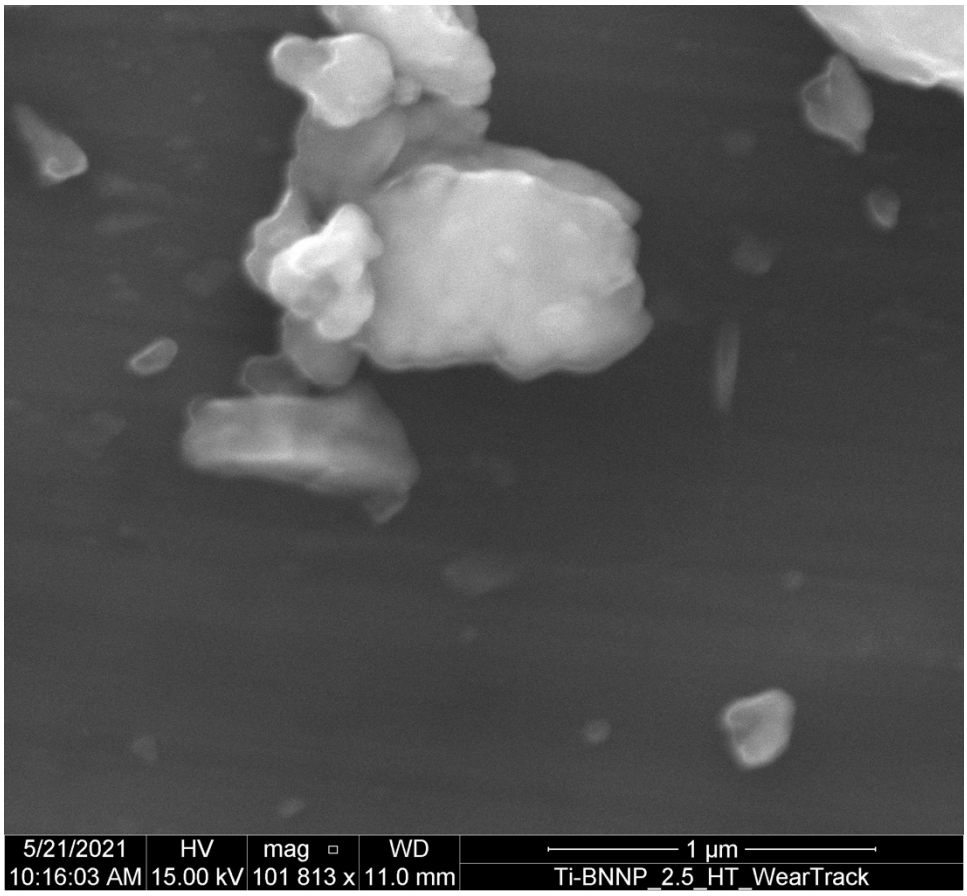

Figure 32. High magnification SEM image of Ti-2.5BN wear track showing intact BNNPs

When looking at the heat-treated Ti-64 sample a large reduction in porosity within the wear tracks can be seen, shown in Figures 33-34. This observation corroborates the reduction in COF experienced by the heat-treated Ti-64 sample. The smooth surface reduces the amount of friction experienced by the ceramic ball, whereas the decrease in pores results in less debris being collected and reintroduced as a wear accelerant. Finally, Figure 34 shows that despite being pure Ti-64, the energy density was low enough for this sample to experience the sample ummelted particles.

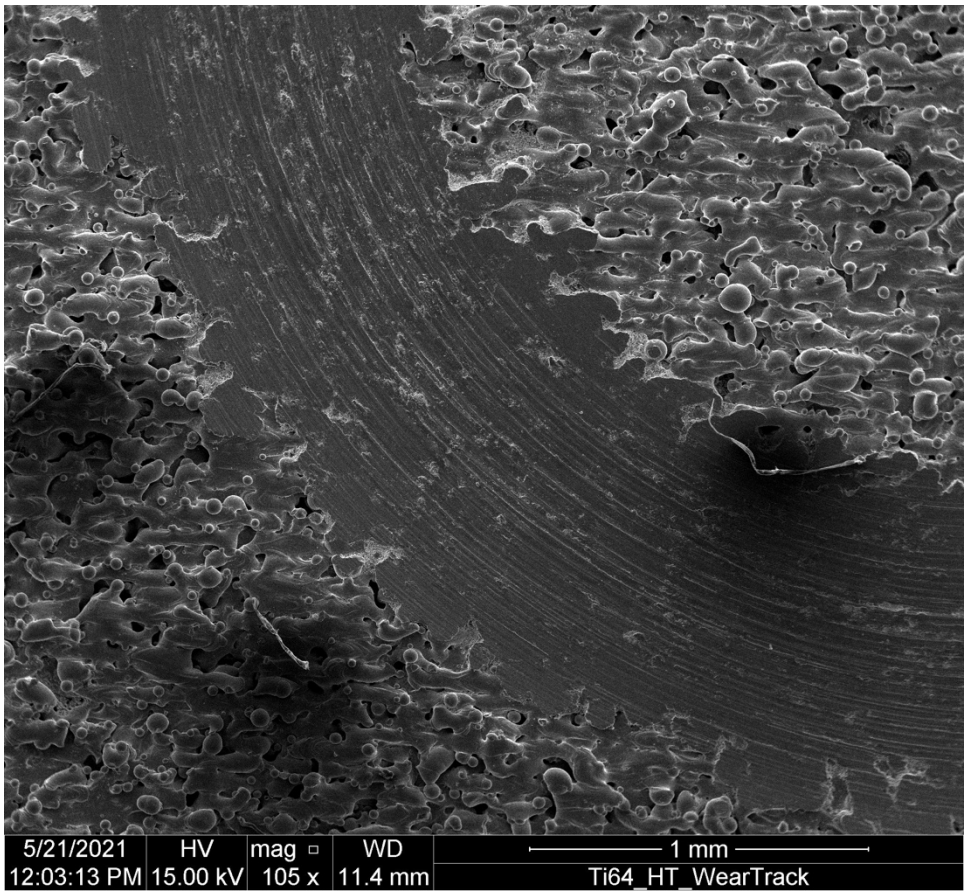

Figure 33. Low Magnification SEM image of Ti-64 heat treated wear track

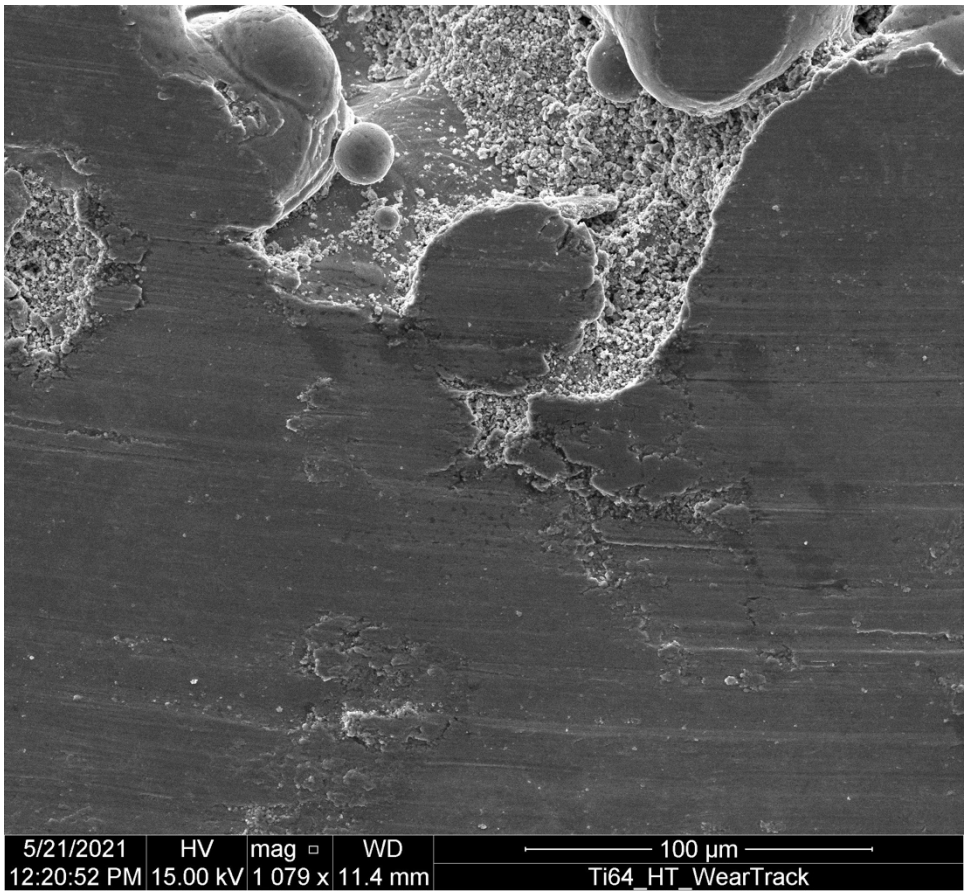

Figure 34. Medium magnification SEM image of Ti-64 heat treated wear track showing unmelted particles and adhesive wearing

THIS PAGE INTENTIONALLY LEFT BLANK

V. CONCLUSION

A. SUMMARY OF RESULTS

Overall, this research confirmed Ti-MMC reinforced with BNNP can be manufactured via SLM. Confirmation is based up successfully printing Ti-BNNP samples using multiple geometries and BNNP compositions. Furthermore, the presence of BN will yield an increase in hardness attributed to both the increase of α' microstructure and the effects of BNNP regions within the matrix. The localized and intrinsic hardness was able to increase by 36%, using the Ti-2.5BN composite despite using a lower energy density that left unmelted particles that caused the formation of pores.

Regarding tribological enhancements, the composite materials showed COF capable of being reduced when BNNP is added to the matrix. The most significant decrease in COF was experienced by the Ti-0.5BN composite, showing an 18% decrease. This confirms the lubrication properties of BNNP because of their two-dimensionality. However, since the wear depth data was obfuscated, further analysis using 3D profilometers would be a more effective way of determining the actual wear depth.

B. FUTURE WORK

1. Optimize Spatial Array Synthesis

Synthesis of composite powders is an area requiring further optimization to produce a HEBM method that modifies parameters based upon volume percent composition. As can be seen, the ball ratio plays key role in the particulate dispersion, formation of large agglomerates and overall flowability of the composite powders. A technique that results in powder morphology that is similar despite the reinforcement composition, is especially important when assessing if the powder is capable of being SLM. Although the spatial arrays allow for better flowability, they still are subject to regional inconsistencies resulting from the deformation of the powders during the HEBM process.

2. Optimize Energy Density

Porosity was another issue experienced when building each part using the SLM. When using and energy density of 60 J/mm^3 the parts experience reactivity which resulted incomplete part fabrication. Despite being able to successfully print all parts researched in thesis, optimizing the laser parameters would be beneficial to manufacturing fully dense parts, without the need to heat treat. Furthermore, by reducing the porosity through laser parameter optimization, enhancements in mechanical properties could be studied without the data being skewed by localized defects.

LIST OF REFERENCES

[1] Manivasagam, G., Dhinasekaran, D., and Rajamanickam, A., 2010, "Biomedical Implants: Corrosion and Its Prevention - A Review," *Recent Pat. Corros. Sci.*, 2(1), pp. 40–54.

[2] Elias, C. N., Lima, J. H. C., Valiev, R., and Meyers, M. A., 2008, "Biomedical Applications of Titanium and Its Alloys," *J. Miner.*, 60(3), pp. 46–49.

[3] Wang, W., and Khoon, C., 2013, "Titanium Alloys in Orthopaedics," *Titanium Alloys - Advances in Properties Control*, J. Sieniawski, ed., InTech, pp. 1–21.

[4] Hermawan, H., Ramdan, D., and P. Djuansjah, J. R., 2011, "Metals for Biomedical Applications," *Biomedical Engineering - From Theory to Applications*, R. Fazel, ed., InTech, pp. 1–23.

[5] Hansen, D. C., 2008, "Metal Corrosion in the Human Body: The Ultimate Bio-Corrosion Scenario," *Electrochem. Soc. Interface*, 17(2), pp. 31–34.

[6] Eliaz, N., 2019, "Corrosion of Metallic Biomaterials: A Review," *Materials*, 12(3), pp. 1–91.

[7] Aniołek, K., Kupka, M., Barylski, A., and Mieszczak, Ł., 2016, "Characteristic of Oxide Layers Obtained on Titanium in the Process of Thermal Oxidation," *Arch. Metall. Mater.*, 61(2), pp. 853–856.

[8] Yi, M., Shen, Z., Zhao, X., Liang, S., and Liu, L., 2014, "Boron Nitride Nanosheets as Oxygen-Atom Corrosion Protective Coatings," *Appl. Phys. Lett.*, 104(14), pp. 1–5.

[9] Wohlers, T., and Caffrey, T., "Additive Manufacturing: Going Mainstream," *Addit. Manuf.*, pp. 1–5.

[10] Zhang, L.-C., and Attar, H., 2016, "Selective Laser Melting of Titanium Alloys and Titanium Matrix Composites for Biomedical Applications: A Review: Selective Laser Melting of Titanium Alloys ...," *Adv. Eng. Mater.*, 18(4), pp. 463–475.

[11] Yadroitsev, I., and Smurov, I., 2010, "Selective Laser Melting Technology: From the Single Laser Melted Track Stability to 3D Parts of Complex Shape," *Phys. Procedia*, 5, pp. 551–560.

[12] Mohammed Maniruzzaman, 2019, *3D and 4D Printing in Biomedical Applications: Process Engineering and Additive Manufacturing*, Wiley-VCH Verlag GmbH & Co., KGaA, Boschstr. 12, 69469 Weinheim, Germany.

[13] Ngo, T. D., Kashani, A., Imbalzano, G., Nguyen, K. T. Q., and Hui, D., 2018, "Additive Manufacturing (3D Printing): A Review of Materials, Methods, Applications and Challenges," *Compos. Part B Eng.*, 143, pp. 172–196.

[14] Hayat, M. D., 2019, "Titanium Metal Matrix Composites_ An Overview," *Compos. Part A*, pp. 418–438.

[15] Cooke, S., Ahmadi, K., Willerth, S., and Herring, R., 2020, "Metal Additive Manufacturing: Technology, Metallurgy and Modelling," *J. Manuf. Process*., 57, pp. 978–1003.

[16] Ponsonnet, L., Reybier, K., Jaffrezic, N., Comte, V., Lagneau, C., Lissac, M., and Martelet, C., 2003, "Relationship between Surface Properties (Roughness, Wettability) of Titanium and Titanium Alloys and Cell Behaviour," *Mater. Sci. Eng. C*, 23(4), pp. 551–560.

[17] Wankhede, S. V., Shinde, S. L., and Wasnik, A. R., 2013, "Modelling of Cu-Al2O3 Metal Matrix Composite Prepared By Powder Metallurgy Route," *Int. J. Eng. Adv. Technol.*, 3(1), pp. 330–332.

[18] Mahmood, M. A., Popescu, A. C., and Mihailescu, I. N., "Metal Matrix Composites Synthesized by Laser-Melting Deposition: A Review," *Materials*, pp. 1–28.

[19] Huang, L. J., Geng, L., and Peng, H.-X., 2015, "Microstructurally Inhomogeneous Composites: Is a Homogeneous Reinforcement Distribution Optimal?," *Prog. Mater. Sci.*, 71, pp. 93–168.

[20] Vaidya, R. U., and Chawla, K. K., 1994, "Thermal Expansion of Metal-Matrix Composites," *Compos. Sci. Technol.*, 50(1), pp. 13–22.

[21] Cai, C., Radoslaw, C., Zhang, J., Yan, Q., Wen, S., Song, B., and Shi, Y., 2019, "In-Situ Preparation and Formation of TiB/Ti-6Al-4V Nanocomposite via Laser Additive Manufacturing: Microstructure Evolution and Tribological Behavior," *Powder Technol.*, 342, pp. 73–84.

[22] Das, M., Patil, S., Bhargava, N., Kang, J.-F., Riedel, L. M., Seal, S., and Hickman, J. J., 2007, "Auto-Catalytic Ceria Nanoparticles Offer

Neuroprotection to Adult Rat Spinal Cord Neurons," *Biomaterial*s, 28(10), pp. 1918–1925.

[23] Anirban, Sk., Paul, T., and Dutta, A., 2015, "Vacancy Mediated Ionic Conduction in Dy Substituted Nanoceria: A Structure–Property Correlation Study," *RSC Adv*., 5(62), pp. 50186–50195.

[24] Hirst, S. M., Karakoti, A. S., Tyler, R. D., Sriranganathan, N., Seal, S., and Reilly, C. M., 2009, "Anti-Inflammatory Properties of Cerium Oxide Nanoparticles," *Small*, 5(24), pp. 2848–2856.

[25] Janoš, P., Hladík, T., Kormunda, M., and Ederer, J., "Thermal Treatment of Cerium Oxide and Its Properties: Adsorption Ability versus Degradation Efficiency," *Adv. Mater. Sci. Eng.*, 2014, pp. 1–12.

[26] Kostoglou, N., Polychronopoulou, K., and Rebholz, C., 2015, "Thermal and Chemical Stability of Hexagonal Boron Nitride (h-BN) Nanoplatelets," *Vacuum*, 112, pp. 42–45.

[27] Nieto, A., Lahiri, D., and Agarwal, A., 2012, "Synthesis and Properties of Bulk Graphene Nanoplatelets Consolidated by Spark Plasma Sintering," *Carbon*, 50(11), pp. 4068–4077.

[28] Kundu, S., Hussain, M., Kumar, V., Kumar, S., and Das, A. K., 2018, "Direct Metal Laser Sintering of TiN Reinforced Ti6Al4V Alloy Based Metal Matrix Composite: Fabrication and Characterization," *Int. J. Adv. Manuf. Technol.*, 97(5–8), pp. 2635–2646.

[29] Attar, H., Löber, L., Funk, A., Calin, M., Zhang, L. C., Prashanth, K. G., Scudino, S., Zhang, Y. S., and Eckert, J., 2015, "Mechanical Behavior of Porous Commercially Pure Ti and Ti–TiB Composite Materials Manufactured by Selective Laser Melting," *Mater. Sci. Eng. A*, 625, pp. 350–356.

[30] Gu, D., Hagedorn, Y.-C., Meiners, W., Wissenbach, K., and Poprawe, R., 2011, "Selective Laser Melting of In-Situ TiC/Ti5Si3 Composites with Novel Reinforcement Architecture and Elevated Performance," *Surf. Coat. Technol*., 205(10), pp. 3285–3292.

[31] Singh, N., Hameed, P., Ummethala, R., Manivasagam, G., Prashanth, K. G., and Eckert, J., 2020, "Selective Laser Manufacturing of Ti-Based Alloys and Composites: Impact of Process Parameters, Application Trends, and Future Prospects," *Mater. Today Adv.*, 8, pp. 1–38.

[32] Kühnle, T., and Partes, K., 2012, "In-Situ Formation of Titanium Boride and Titanium Carbide by Selective Laser Melting," *Phys. Procedia*, 39, pp. 432–438.

[33] Attar, H., Bönisch, M., Calin, M., Zhang, L.-C., Scudino, S., and Eckert, J., 2014, "Selective Laser Melting of in Situ Titanium–Titanium Boride Composites: Processing, Microstructure and Mechanical Properties," *Acta Mater.*, 76, pp. 13–22.

[34] Ahmed, M., Pasha, M., Nan, W., and Ghadiri, M., 2020, "A Simple Method for Assessing Powder Spreadability for Additive Manufacturing," *Powder Technol.*, 367, pp. 671–679.

[35] Luo, S., Song, T., Liu, B., Tian, J., and Qian, M., 2019, "Recent Advances in the Design and Fabrication of Strong and Ductile (Tensile) Titanium Metal Matrix Composites," *Adv. Eng. Mater.*, 21(7), pp. 1–13.

[36] Cai, C., He, S., Li, L., Teng, Q., Song, B., Yan, C., Wei, Q., and Shi, Y., 2019, "In-Situ TiB/Ti-6Al-4V Composites with a Tailored Architecture Produced by Hot Isostatic Pressing: Microstructure Evolution, Enhanced Tensile Properties and Strengthening Mechanisms," *Compos. Part B Eng.*, 164, pp. 546–558.

[37] Fousova, M., and Vojtech, D., 2018, "Thermal Treatment of 3D-Printed Titanium Alloy," *Manuf. Technol.*, 18(2), pp. 227–232.

[38] Roudnicka, M., Mertova, K., and Vojtech, D., 2019, "Influence of Hot Isostatic Pressing on Mechanical Response of As-Built SLM Titanium Alloy," *IOP Conf. Ser. Mater. Sci. Eng.*, 629, pp. 1–7.

[39] He, J., Li, D., Jiang, W., Ke, L., Qin, G., Ye, Y., Qin, Q., and Qiu, D., 2019, "The Martensitic Transformation and Mechanical Properties of Ti6Al4V Prepared via Selective Laser Melting," *Materials*, 12(2), pp. 1–14.

[40] William D. Callister Jr., David G. Rethwisch, *Materials Science and Engineering AN INTRODUCTION*, John Wiley & Sons, Inc.

[41] Vrancken, B., Thijs, L., Kruth, J.-P., and Van Humbeeck, J., 2012, "Heat Treatment of Ti6Al4V Produced by Selective Laser Melting: Microstructure and Mechanical Properties," *J. Alloys Compd.*, 541, pp. 177–185.

[42] Vrancken, B., Thijs, L., Kruth, J.-P., and Van Humbeeck, J., 2014, "Microstructure and Mechanical Properties of a Novel β Titanium Metallic Composite by Selective Laser Melting," *Acta Mater*., 68, pp. 150–158.

[43] Yining He, Colt Montgomery, Jack Beuth, Bryan Webler, "Melt Pool Geometry and Microstructure of Ti6Al4V with B Additions Processed by Selective Laser Melting Additive Manufacturing | Elsevier Enhanced Reader," *Mater. Des.*, 183(2019), pp. 1–13.

[44] Jiang, L., Yang, H., Yee, J. K., Mo, X., Topping, T., Lavernia, E. J., and Schoenung, J. M., 2016, "Toughening of Aluminum Matrix Nanocomposites via Spatial Arrays of Boron Carbide Spherical Nanoparticles," *Acta Mater.*, 103, pp. 128–140.

[45] Jiang, L., Wen, H., Yang, H., Hu, T., Topping, T., Zhang, D., Lavernia, E. J., and Schoenung, J. M., 2015, "Influence of Length-Scales on Spatial Distribution and Interfacial Characteristics of B4C in a Nanostructured Al Matrix," *Acta Mater.*, 89, pp. 327–343.

[46] Shaikh, A., Kumar, S., Dawari, A., Kirwai, S., Patil, A., and Singh, R., 2019, "Effect of Temperature and Cooling Rates on the A+β Morphology of Ti-6Al-4V Alloy," *Procedia Struct. Integr.*, 14, pp. 782–789.

[47] Amanov, A., 2021, "Tribology of Ti-6Al-4V Alloy Manufactured by Additive Manufacturing," *Tribology in Materials and Manufacturing - Wear, Friction and Lubrication*, A. Patnaik, T. Singh, and V. Kukshal, eds., IntechOpen, pp. 1–16.

THIS PAGE INTENTIONALLY LEFT BLANK

INITIAL DISTRIBUTION LIST

1. Defense Technical Information Center
   Ft. Belvoir, Virginia

2. Dudley Knox Library
   Naval Postgraduate School
   Monterey, California